ACCSCIENCE PUBLISHING

International Journal of Bioprinting

ACCEPTED PAPER · MAIN TEXT

Stimuli-responsive bioinks for bioprinted cancer models: Toward personalized drug screening and resistance modeling

Paper version: Accepted Paper

Accepted Papers are manuscripts accepted for publication, encompassing all changes made following the peer review process, along with a standard cover page indicating the paper version and an "Accepted Paper" watermark, but excluding any other editing, typesetting or other changes made by AccScience Publishing and/or authors post-acceptance.

Article ID: IJB026350377

Citation: Zeng J, Ni WJ. Stimuli-responsive bioinks for bioprinted cancer models: Toward personalized drug screening and resistance modeling. *Int J Bioprint*. 2026. doi: 10.36922/IJB026350377

Copyright: © 2026 Author(s). This is an Open Access article distributed under the terms of the Creative Commons Attribution License, permitting distribution, and reproduction in any medium, provided the original work is properly cited.

Publisher's Note: AccScience Publishing remains neutral with regard to jurisdictional claims in published maps and institutional affiliations.

AccScience Publishing
REVIEW ARTICLE
Volume X Issue X (2026)

doi: 10.36922/IJB026350377

Stimuli-responsive bioinks for bioprinted cancer models: Toward personalized drug screening and resistance modeling

Running title: Stimuli-responsive bioinks for cancer models

Jing Zeng[1]* and Wei-Jian Ni [2,3]*

[1] Department of Pharmacy, Wenzhou People's Hospital, The Third Affiliated Hospital of Shanghai University, Wenzhou, Zhejiang, 325000, China

[2] Department of Pharmacy, The First Affiliated Hospital of USTC, Division of Life Sciences and Medicine, University of Science and Technology of China, Hefei, Anhui, 230001, China

[3] Centre for Leading Medicine and Advanced Technologies of IHM, The First Affiliated Hospital of USTC, Division of Life Sciences and Medicine, University of Science and Technology of China, Hefei, Anhui, 230001, China

***Corresponding authors:**

Jing Zeng (1310370765@qq.com)

Wei-Jian Ni (niweijian@ustc.edu.cn)

Citation: Zeng J, Ni WJ. Stimuli-responsive bioinks for bioprinted cancer models: Toward personalized drug screening and resistance modeling. *Int J Bioprint*. 2026. doi: 10.36922/IJB026350377

ACCEPTED PAPER

Received: August 27, 2026
Revised: September 21, 2026
Accepted: September 22, 2026
Published online: September 24, 2026

Copyright: © 2026 Author(s). This is an Open Access article distributed under the terms of the Creative Commons Attribution License, permitting distribution, and reproduction in any medium, provided the original work is properly cited.

Publisher's Note: AccScience Publishing remains neutral with regard to jurisdictional claims in published maps and institutional affiliations.

ACCEPTED PAPER

Abstract

Drug resistance remains the leading cause of treatment failure in solid tumors. Conventional two-dimensional (2D) cultures and animal models cannot reproduce the dynamic tumor microenvironment (TME) cues driving resistance evolution—matrix stiffening, acidification, hypoxia, and enzymatic remodeling. Most 3D-bioprinted constructs remain static matrices and share this limitation. This review proposes the spatiotemporal dynamics of the TME as a design criterion for stimuli-responsive ("smart") bioinks, whose stiffness, degradability, drug-release kinetics, and geometry change in response to endogenous TME cues or external triggers. This review distills the TME into a quantitative design blueprint; examines the printability, cytocompatibility, and responsiveness requirements of smart inks, together with the dynamic chemistries enabling them; and summarizes strategies for reconstructing an evolving TME, using pancreatic ductal adenocarcinoma and glioblastoma as anchor case studies. The scope is restricted to cancer modeling and drug screening, excluding drug delivery and tissue regeneration. Current evidence remains proof-of-concept: printed models recapitulate resistance-associated phenotypes such as stiffness-mediated chemoresistance, cancer stem cell enrichment, dormancy, and phenotypic plasticity, whereas prospective validation of resistance models in patients has not been achieved. This review outlines the path from phenotype recapitulation to clinical prediction and analyzes prerequisites including vascularization, standardization, regulatory translation, and artificial intelligence (AI)-guided ink design.

Keywords: 3D bioprinting; Stimuli-responsive bioink; Tumor microenvironment; Drug screening; Drug resistance; Patient-derived tumor models

ACCEPTED PAPER

1. Introduction

1.1 Limitations of conventional cancer models

The predictive failure of current preclinical models is a well-documented bottleneck in oncology drug development. The majority of oncology compounds entering clinical trials fail, in large part because efficacy signals generated in 2D culture and in animal models do not translate to patients[1,2]. Two-dimensional monolayer cultures deprive cancer cells of extracellular matrix (ECM) ligands, three-dimensional cell–cell contacts, and the nutrient–oxygen gradients that define in vivo physiology. As a result, drug sensitivity measurements are systematically distorted, and half-maximal inhibitory concentrations (IC50) are frequently underestimated[1,3]. Animal models provide systemic context but suffer from interspecies differences in pharmacokinetics and immunity, high cost, and limited throughput. Patient-derived xenografts (PDX) further carry the confounder of a chimeric human–mouse microenvironment, in which the stromal and immune compartments are of murine origin and only partially recapitulate the human tumor–host interface[3,4].

Patient-derived organoids (PDOs) have markedly improved clinical relevance. Retrospective and prospective studies have demonstrated concordance between organoid drug response and patient outcome in gastric, lung, colorectal, and bladder cancers[5-8]. However, PDO culture in animal-derived Matrigel is hampered by batch-to-batch variability, ill-defined biochemical composition, and, critically, the absence of stromal, vascular, and immune compartments and of the dynamic physical signals that shape drug response[9-11]. Moreover, most organoid platforms culture cells in static, proteinaceous drops whose mechanical and chemical properties are neither controlled nor representative of the tumor from which the cells were derived[11,12]. These limitations motivate the search for engineered matrices and fabrication strategies that can embed patient-derived cells within defined, tunable, and, decisively, dynamic microenvironments[12,13]. Nevertheless, the demonstrated clinical concordance of organoid-based drug testing establishes a powerful precedent. If organoids cultured in

ACCEPTED PAPER

undefined matrices and largely without dynamic cues can already predict response, engineered models with controlled, dynamic microenvironments should perform substantially better[5,14,15].

1.2 The rise of 3D bioprinting for cancer modeling

3D bioprinting resolves several of these limitations by depositing cells and biomaterials in spatially controlled, reproducible geometries at throughputs compatible with screening[2,16,17]. Bioprinted cancer models now integrate multiple cell types, including cancer cells, cancer-associated fibroblasts (CAFs), macrophages, and endothelial cells, within engineered ECM mimics, enabling the construction of vascularized tumor arrays, patient-derived constructs, and multicellular tumor microenvironments[18-21]. The bioink is the decisive determinant of model fidelity: it must simultaneously satisfy printability, cytocompatibility, and the capacity to present biochemical and biophysical cues that mimic the native tumor niche[1,2,17]. Advances in embedded printing, volumetric bioprinting, and suspension baths have progressively widened the window of printable ink chemistries, allowing softer and more biologically faithful matrices to be shaped into complex architectures[22-24]. The technology has matured to the point that patient-derived tissue models and multicellular glioma models can be produced reproducibly. While whole-organ-scale constructs have been demonstrated as proofs of concept, their routine and reproducible production remains an open engineering challenge. Recent assessments of the state of the art converge on the same conclusion: the remaining bottleneck is not fabrication itself but the fidelity of the ink–biology interface[25,26] (Figure 1C).

1.3 Why responsiveness is the key missing dimension

The TME is not a static scaffold but a dynamic, evolving ecosystem.

Tumor progression and therapy itself continuously perturb the microenvironment. Chemotherapy and radiotherapy intensify hypoxia and oxidative stress[27,28],while desmoplastic reactions stiffen the ECM[29,30]. In parallel, lysyl oxidase (LOX)-mediated

ACCEPTED PAPER

crosslinking and matrix metalloproteinase (MMP) remodeling continuously reshape the matrix[31,32], and immune cells are progressively re-educated toward immunosuppressive states[33,34]. Static models capture only a single snapshot of this trajectory and therefore miss the process by which resistance emerges[12,35]. Stimuli-responsive ("smart") bioinks, which are engineered to respond to endogenous TME cues or external triggers, provide this missing dynamic dimension. They convert printed tumor models from passive scaffolds into adaptive systems that can recapitulate the evolution of resistance-associated phenotypes[12,36]. This responsiveness is not an engineering nicety but a biological necessity. Because resistance is a time-dependent adaptation rather than a fixed property, only models that change over time can capture the emergence of resistance[12,29]. To address this gap, this review distinguishes three levels of evidence: (i) recapitulation of resistance-associated phenotypes, (ii) retrospective correlation between model readouts and clinical response, and (iii) prospective clinical prediction of resistance. Current bioprinted cancer models operate predominantly at level (i); level (ii) is emerging from the organoid literature; level (iii) remains a goal to be achieved. This temporal perspective also reframes what a predictive experiment should measure: instead of a single endpoint after a fixed incubation, the informative output is the trajectory, that is, when sensitivity erodes, how quickly it erodes, and under which environmental conditions[37,38].

1.4 Scope and structure of this review

This review focuses specifically on stimuli-responsive bioinks for bioprinted cancer models, with applications centered on drug screening and resistance modeling rather than drug delivery or tissue regeneration. This review first defines the TME as a design blueprint for smart inks (Section 2) and then examines the fundamentals of smart bioink design and dynamic chemistry (Section 3). Section 4 systematically classifies stimuli-responsive mechanisms, and Section 5 describes strategies for recapitulating the dynamic TME. Section 6 analyzes applications in drug screening and resistance modeling, using PDAC and GBM as anchor case studies. Finally, Section 7 addresses

ACCEPTED PAPER

challenges and future perspectives, including standardization, AI-guided ink design, and clinical translation. Throughout, this review prioritizes mechanistic logic over exhaustive citation and emphasizes the criteria by which specific responsive chemistries should be selected for specific biological questions.

2. The Tumor Microenvironment as a Design Blueprint for Smart Bioinks

2.1 Composition and dynamic signal landscape of the TME

The TME comprises cancer cells embedded in a cellular ecosystem of CAFs, tumor-associated macrophages (TAMs) and myeloid cells, T cells, natural killer cells, endothelial cells, and pericytes, all organized within a remodeled ECM[4,39]. CAFs are the principal architects of desmoplasia. They deposit and crosslink collagen while secreting growth factors, chemokines, and metabolites that sustain tumor growth and shield tumor cells from therapy[39,40]. TAMs and myeloid cells populate the tumor stroma at high densities and undergo spatiotemporally regulated polarization states that generally converge toward immunosuppressive and protumoral phenotypes as the tumor evolves[34]. Functionally, the TME is defined by a distinctive spectrum of physicochemical signals. Matrix stiffness spans roughly 0.1-50 kPa with tumor-grade-dependent stiffening, accompanied by increased viscoelasticity and stress relaxation. This envelope spans multiple tumor types; tissue-specific stiffness ranges differ (see Section 2.4). Further hallmarks include extracellular acidosis (pH 6.5-6.9) driven by the Warburg effect, hypoxia with pO2 values approaching 1%, and elevated reactive oxygen species (ROS). Finally, MMP overexpression, ongoing ECM turnover, and elevated interstitial fluid pressure complete this signal landscape[4,35,41] (Figure 1A). Importantly, these signals are not static constants but fluctuate in space and time, during invasion, in response to therapy, and as the tumor evolves, making the TME a moving target that any faithful in vitro model must track[12,34]. These dynamics are spatially organized as well as temporal: stiffness, hypoxia, and immune infiltration vary from

ACCEPTED PAPER

tumor core to invasive front, and the gradients themselves, not just their endpoints, carry biological information that instructs migration, dormancy, and therapy evasion[35,41].

2.2 Resistance mechanisms and the fidelity requirements they impose

Drug resistance arises through two broad, interwoven routes. The first route is TME-mediated resistance, which includes CAF-secreted factors and matrix remodeling that shield tumor cells, TAM polarization toward protumoral states, and mechanotransductive signaling by which matrix stiffening activates YAP/TAZ and integrin-dependent pathways that promote survival under cytotoxic challenge. Physical matrix barriers further limit drug penetration, and increased stiffness has been directly linked to chemotherapy resistance in patient-derived pancreatic cancer organoids . The mechanical dimension deserves emphasis: mechanotransduction is not auxiliary to pharmacology but can be dominant, as illustrated by studies in which matrix stiffness alone determined the difference between drug-sensitive and drug-resistant states[39,42]. The second route is intrinsic resistance, which encompasses CSC enrichment, cellular dormancy, and phenotypic plasticity, that is, the lineage switching and state transitions that allow tumor cells to survive therapy and re-emerge[43,44]. CSCs reside in specialized niches whose mechanical and biochemical properties differ from those of the bulk tumor, and dormancy is controlled by microenvironmental signals that are poorly represented in conventional culture[44-46]. Spatially, resistance-prone phenotypes are often confined to distinct subregions, such as hypoxic cores, invasive rims, or perivascular niches, so the model must be able to localize these states, not merely detect their presence[18,47].

Importantly, resistance is an acquired, time-dependent phenotype: the same tumor that responds to a drug may evolve resistance over weeks, and the microenvironment co-evolves with it[12,33]. A predictive in vitro model must therefore reproduce this dynamic evolution rather than merely report a static phenotype, which is precisely the capability that smart bioinks can confer. The fidelity requirements are consequently

ACCEPTED PAPER

severe. The model must (i) present the correct initial biochemical and mechanical cues and (ii) allow those cues to change over time in a biologically matched manner. It must also (iii) support the readouts needed to detect the emergence of resistance-viability, phenotype, dormancy, and stemness-rather than only its endpoint[12,48].

2.3 Spatiotemporal dynamics as a unifying design framework

Static hydrogels present a fixed stiffness, a uniform chemistry, and a single release profile; they cannot model mechanical memory, dose-accumulation effects, or therapy-induced remodeling[12,35]. Dynamic and four-dimensional (4D) materials, whose properties change over time in response to programmed or environmental triggers, provide the conceptual framework needed to close this gap[49,50]. Within this framework, three design axes emerge: the time axis (when and how fast a property changes), the space axis (where in the construct the change occurs), and the reversibility axis (whether the change is permanent or recoverable)[12,36]. Mechanical memory, that is, the persistence of a phenotype after the mechanical stimulus is removed, adds a fourth consideration: even transient stiffening can leave lasting epigenetic traces, so the history of the matrix matters as much as its instantaneous state[12,35].

2.4 Design blueprint summary: matching response windows to biology

The blueprint distilled from the TME is simple but exacting: the response threshold of a smart bioink must fall within the physiological–pathological window of the corresponding TME signal. For pH-responsive systems, the working window must bracket the interstitial pH of 6.5–6.9 rather than the strongly acidic endolysosomal range used in drug delivery[51]. Enzyme-responsive systems must respond to MMP concentrations actually present in the modeled tumor[32,52]. Stiffness-changing systems should span the 0.1–50 kPa range and match the kinetics of fibrosis[29,53]. Finally, the reversibility of the response must be matched to the dynamics of the process being modeled[12,36.]Reversible and irreversible responses represent different biological processes rather than interchangeable design options. An irreversible change cannot be

ACCEPTED PAPER

recovered within the culture period, and when its mechanical outcome is stiffening it reproduces the sustained, non-resolving stiffening of desmoplastic stroma. Such stiffening is progressive, which makes irreversible systems the appropriate choice for studies of acquired chemoresistance and mechanical memory[29,31]. A reversible system instead represents biology that recovers: transient therapy-induced changes in matrix mechanics, or cyclic mechanical fluctuation during growth and invasion. The relevant distinction is therefore which disease process is modeled, rather than whether switching is convenient. Progressive fibrosis requires a one-way transition, whereas a treatment-induced change that resolves requires recoverable switching[12,53,54.] Where a single model must contain both, the construct requires chemistry that is irreversible in one region and reversible in another, a requirement that current inks satisfy only partially. Two qualifications apply to these windows. First, because the 0.1–50 kPa envelope spans multiple tumor types, the working range must be tumor-type-specific: normal brain parenchyma (~0.1–1 kPa) and pancreatic islets (~1–4 kPa) define the lower end, whereas desmoplastic PDAC (~10–50 kPa) and glioblastoma foci (~5–20 kPa) define the upper end. Second, interstitial pH is spatially heterogeneous within a single construct, where the proliferating, poorly perfused core and the quiescent rim may differ by 0.3–0.5 pH units, so a pH-responsive window must bracket the interstitial range rather than a single averaged value. It is worth emphasizing a deliberate divergence from drug-delivery practice.

In delivery systems, the goal is to concentrate payload at the tumor. In predictive screening, the goal is instead to reproduce the very conditions under which therapy fails. The same chemistries are therefore intentionally used to recreate, rather than to avoid, the hostile microenvironment[36,55].

ACCEPTED PAPER

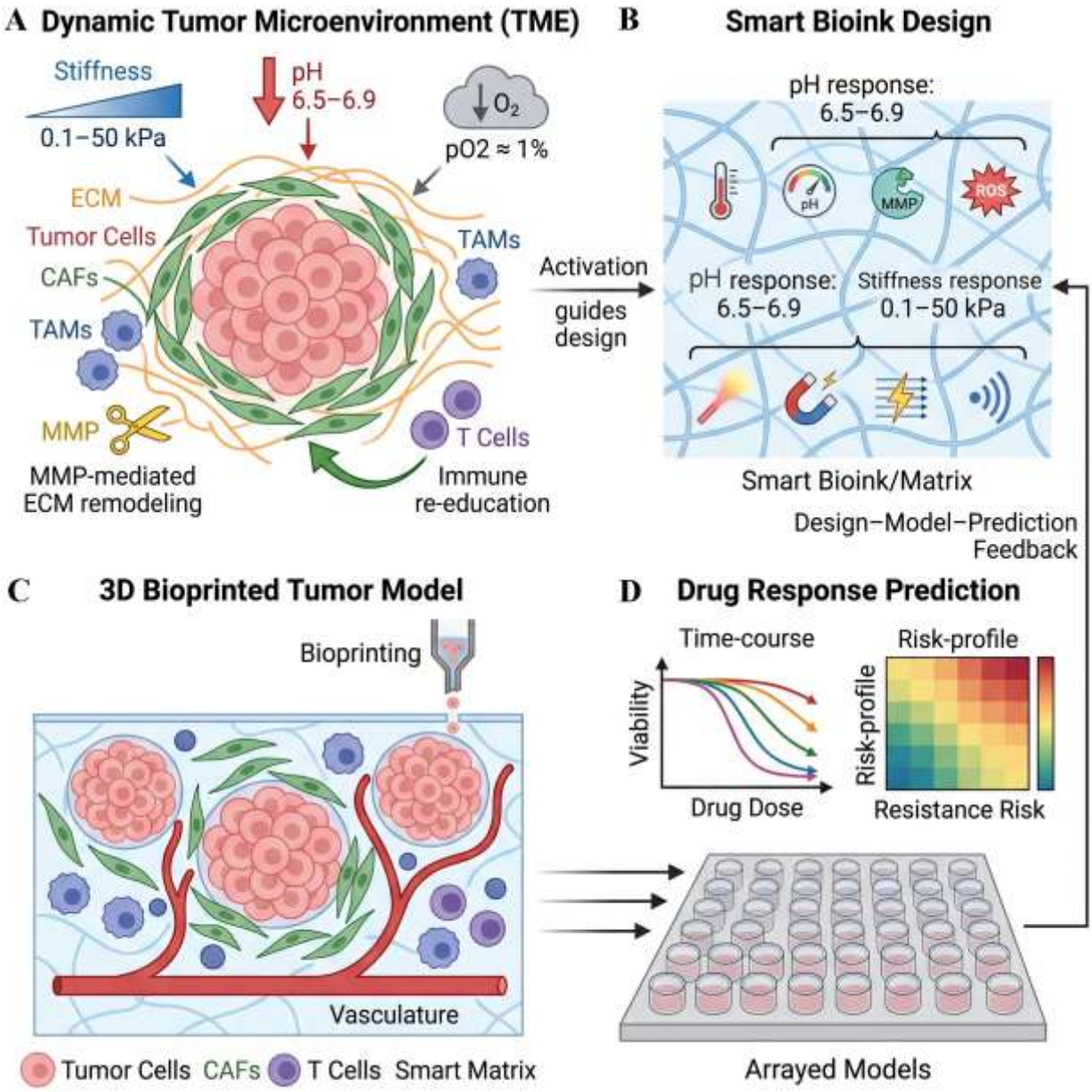


Figure 1. From dynamic tumor microenvironments to predictable drug response. A, The tumor microenvironment (TME) is a dynamic physicochemical ecosystem. Key endogenous signals include matrix stiffening (0.1–50 kPa, a range spanning multiple tumor types; tissue-specific anchors are given in Section 2.4) driven by desmoplastic reactions, extracellular acidosis (pH 6.5–6.9) arising from aerobic glycolysis, hypoxia/oxidative stress with partial pressure of oxygen (pO_2) ≈ 1%, matrix metalloproteinase (MMP)-mediated extracellular matrix (ECM) remodeling, and immune re-education involving cancer-associated fibroblasts (CAFs), tumor-associated macrophages (TAMs) and T cells. B, These signals guide the design of smart bioinks that respond to temperature, pH, enzymes, redox/reactive oxygen species (ROS), light, magnetic/electric/ultrasound fields, or multi-stimuli logic gates, with response windows matched to pathophysiological ranges. C, Patient-derived tumor cells combined with smart matrices are bioprinted into multicellular constructs containing tumor spheroids, stroma, vasculature and

immune cells. D, Arrayed models enable drug screening and resistance modeling through time-resolved dose–response trajectories and risk profiling, closing the design–model–prediction feedback loop.

3. Fundamentals of Smart Bioink Design for Cancer Bioprinting

3.1 Design principles: the printability–cytocompatibility–responsiveness triangle

A functional smart bioink must satisfy three mutually constraining requirements. The first is printability, which encompasses shear-thinning behavior, rapid gelation, and shape fidelity after deposition. The second is cytocompatibility, which requires minimal cytotoxicity during printing and culture as well as appropriate cell-adhesion ligands. The third is responsiveness, which demands a well-defined, tunable response to the target stimulus within the biologically relevant window. These three vertices are in tension. Higher crosslink density improves shape fidelity but restricts dynamic remodeling and cell spreading. Adding responsive groups can perturb rheology and printability, and every chemical modification carries a potential toxicity cost[1,2,36]. Rational design therefore begins with a precise statement of the biological question. The required stiffness range, degradation kinetics, and stimulus window follow from that statement; only then are the polymer backbone and crosslinking chemistry selected[2,12].

Stimuli fall into two categories, each with distinct implications for model design. Endogenous TME signals, including pH, enzymes, ROS, and oxygen, are intrinsic to the tumor. They enable self-regulated responses that mimic physiological feedback, so the model behaves autonomously as the biology dictates[36,51]. Exogenous triggers include temperature, light, magnetic fields, ultrasound, and electrical stimuli. These allow the operator to program responses on demand, decoupling the stimulus from the biology of the model and enabling hypothesis-driven perturbation experiments. The most sophisticated inks combine both: endogenous signals for autonomous behavior, exogenous triggers for user-defined perturbations (Figure 1B). This hybrid architecture

ACCEPTED PAPER

mirrors the logic of the TME itself, in which intrinsic signals and externally imposed stresses such as therapy and hypoxia jointly drive adaptation[36,56].

3.2 Natural polymer systems

Natural polymers dominate cancer bioprinting because of their inherent bioactivity and ECM-like signaling. Gelatin methacryloyl (GelMA) is the most widely used photocrosslinkable ink. Its thermo-gelation and UV/visible-light crosslinking give tunable stiffness over a broad range, making it the workhorse for organotypic tumor models[2,57]. GelMA also tolerates reinforcement with nanomaterials such as Laponite, which adjusts rheology and stiffness while retaining cytocompatibility, and it supports patient-derived cells and stromal components[18,57]. Sodium alginate crosslinks rapidly and reversibly through ionic interactions. It provides excellent print fidelity and serves well as a sacrificial or support system, although it lacks cell-adhesion motifs and shows weak mechanical performance[2,58]. Collagen and gelatin recapitulate native ECM ligands and self-assemble into fibrillar networks. Printing them at low concentration, however, demands support strategies such as FRESH or embedded printing in suspension baths[22,24]. Hyaluronic acid (HA) engages CD44 signaling relevant to cancer stemness and can be functionalized for controlled crosslinking, which makes it a versatile component of composite inks. Its viscoelastic properties can also be tuned toward tumor-like stress relaxation[59-61]. Matrigel and decellularized ECM (dECM) bioinks offer the highest biochemical fidelity and tissue-specific cues, but they suffer from batch variability and poor printability. Increasingly refined dECM-based inks preserve organ-specific signaling for liver, breast, and brain models[9,62,63.] A recurring theme across natural systems is the trade-off between biological fidelity and experimental control, which motivates hybrid and synthetic formulations[9,36]. For screening purposes, composite designs are becoming the standard: they pair the bioactivity of natural polymers with the mechanical definition of synthetic or nanomaterial components. Bioprinted ovarian cancer peritoneal spheroid models engineered for immunomodulatory compound testing illustrate the approach[57,64].

ACCEPTED PAPER

3.3 Synthetic and composite systems

Synthetic polymers offer a chemically defined, inert background onto which biofunctionality can be grafted orthogonally. Poly(ethylene glycol) (PEG) hydrogels are biocompatible, and their degradation can be programmed through degradable linkers. This programmability allows biochemical and mechanical cues to be decoupled systematically, an essential feature for establishing causal relationships between matrix properties and drug response[2,9]. Temperature-responsive polymers such as poly(N-isopropylacrylamide) (PNIPAM, lower critical solution temperature ~32 °C) and Pluronic F127 undergo sol–gel transitions near physiological temperature. Pluronic is commonly employed as a sacrificial ink to form vascular channels, while PNIPAM-based dual-gelling inks paired with thermoreversible support baths achieve high-resolution printing[65-67]. Composite and interpenetrating networks reinforced with nanomaterials such as Laponite, cellulose nanofibrils, or nanoparticles simultaneously improve print resolution and mechanical performance while preserving cytocompatibility[57,68,69]. The synthetic path also enables precise presentation of adhesive ligands such as RGD and GFOGER at controlled densities. The biochemical background can therefore be titrated independently of mechanics[2,9]. Support and embedding media further expand the printable window. Gelatin-based and polysaccharide-based suspension baths allow soft, biologically faithful inks to be shaped without the rheological constraints of free-form extrusion. Versatile embedding media offering multiple crosslinking modes extend this flexibility further[22,70].

3.4 Dynamic chemistry as the molecular origin of responsiveness

The responsiveness of smart inks originates at the molecular level from dynamic bonds and supramolecular interactions. Dynamic covalent bonds, including hydrazone/oxime, boronate ester, imine (Schiff base), and disulfide linkages, are reversible, exchangeable, and stimulus-sensitive. They provide the molecular machinery for pH-, ROS-, or enzyme-triggered gel degradation and stiffness changes[71-73]. In a representative study,

ACCEPTED PAPER

hydrazone-crosslinked hydrogels were printed by FRESH methods, showing that dynamic chemistries are compatible with high-fidelity fabrication[71]. Boronate ester hydrogels illustrate the importance of pKa matching. The responsive window is set by the equilibrium between boronate ester formation and hydrolysis. That equilibrium must be tuned to the pH of the tumor interstitium[72]. Small-molecule modulators of dynamic bond exchange have further been used to control the gelation kinetics of printed hydrogels, adding a chemical dial to printing protocols[73]. Supramolecular interactions, including host–guest pairs such as cyclodextrin–adamantane, hydrogen bonding, and metal coordination, confer self-healing and shear-thinning behavior. Extrusion printing directly exploits these properties, which also maintain construct integrity under mechanical stress[61,74,75]. The viscoelasticity and stress relaxation arising from these dynamic bonds regulate cell phenotype, including spreading, proliferation, and mechanosensitive gene expression. These effects operate through mechanisms distinct from static stiffness and add an essential variable to the design space[12,53,76]. Dynamic bond exchange likewise underpins the self-healing behavior that preserves printed architecture under repeated mechanical perturbation. Hydrogel systems exploit this property while simultaneously delivering regenerative or immunomodulatory cues[74,75]. For cancer models specifically, matrix viscoelasticity has been shown to modulate invasion and mechanotransduction in ways that static stiffness alone cannot predict[53,76].

3.5 Influence of printing technology on responsive ink design

The choice of printing technology constrains ink chemistry. Extrusion printing favors shear-thinning, rapidly gelling inks and tolerates temperature-sensitive systems whose nozzles are thermostatted[67,73]. Digital light processing (DLP) and volumetric printing require photoactive inks with adequate light penetration and manageable free-radical toxicity. Volumetric bioprinting has been successfully combined with dECM-derived inks to fabricate centimeter-scale constructs rapidly[23,77]. Embedded and FRESH printing in suspension baths enable soft, low-concentration inks that better mimic native

ACCEPTED PAPER

tissue mechanics[22,24]. Each technology also imposes a characteristic trade-off between resolution, throughput, and achievable stiffness range. The printing platform and the ink chemistry must therefore be co-designed rather than selected independently[23,25]. These technological considerations are summarized in Table 1, which compares the major ink systems used in cancer bioprinting.

Table 1. Comparison of major bioink systems for cancer bioprinting

Material	Crosslinking mechanism	Origin of responsiveness	Representative cancer model applications	Key limitations
GelMA	Photo-crosslinking (methacrylate, 365 nm radical initiation)	Photodegradation; tunable stiffness; enzymatic degradation by gelatinase	Breast cancer organoids; GBM models; melanoma spheroids; multi-celltype constructs	Radical toxicity during crosslinking; batch-dependent methacrylation degree; limited print resolution
Alginate	Ionic (Ca^{2+}) crosslinking; reversible by chelation	Ion exchange; mechanical tunability (0.1–100 kPa); shear-thinning	Multi-celltype tumor models; hepatocellular carcinoma; drug-release scaffolds; encapsulated spheroids	Poor cell adhesion (no native RGD unless modified); slow degradation; limited biological signaling
Collagen / gelatin	Enzymatic (transglutaminase), chemical (EDC/NHS), or	MMP-degradable; temperature-dependent gelation;	Invasion assays; breast cancer; pancreatic cancer desmoplasia	Batch variability; weak mechanical strength; rapid contraction;

	physical (temperature gelation)	native cell-adhesion motifs	models; dermal equivalents	temperature-sensitive printing window
Hyaluronic acid (HA)	Photo-crosslinking (methacrylated HA); click chemistry (thiol-ene); dynamic hydrazone	CD44-mediated uptake; hyaluronidase degradation; tunable stiffness and charge	Glioma (CD44-high); breast cancer; drug-delivery platforms; chondrosarcoma	High cost; viscous solutions complicate extrusion; slow gelation kinetics; limited cell adhesion
Matrigel and dECM	Temperature gelation (Matrigel); self-assembly (dECM); often combined with chemical crosslinkers	Temperature; MMP degradation; native growth-factor reservoir; tissue-specific ECM composition	PDOs (organoids); PDAC; colorectal; prostate; liver cancer; most biologically faithful models	Batch-to-batch variability; undefined composition; xenogeneic origin (Matrigel); limited mechanical tunability; high cost
PEG	Photo-crosslinking (acrylate); click chemistry; dynamic covalent (disulfide, hydrazone)	Programmable degradation (ester, enzymatic); tunable stiffness independent of bioactivity	Mechanobiology studies; stiffness-mediated drug-resistance models; spheroid culture; synthetic matrices	Bioinert (requires conjugated RGD or peptides); non-degradable backbone unless specifically designed; limited cell spreading

PNIPAM / Pluronic	Physical (temperature-induced micelle packing, LCST ~32 °C)	Temperature (LCST/UCST); reversible sol–gel transition; thermally triggered release	On-demand cell harvesting; temperature-triggered drug release; injectable scaffolds; thermo-responsive coatings	Cytotoxic at high concentration; limited mechanical strength; non-degradable; narrow temperature window; leaching risk
Composite / nanoreinforced	Hybrid (polymer + nanoparticles: clay, cellulose nanocrystals, magnetic NPs, graphene oxide)	Multi-modal (mechanical + magnetic + thermal); shear-thinning; self-healing; conductivity	Complex tissue constructs; anisotropic tumor models; magnetic actuation; electro-active scaffolds; bone metastasis	Nanoparticle cytotoxicity and agglomeration; complex characterization; regulatory concerns; batch reproducibility; clearance

Abbreviations: dECM, decellularized extracellular matrix; ECM, extracellular matrix; EDC/NHS, 1-ethyl-3-(3-dimethylaminopropyl)carbodiimide/N-hydroxysuccinimide; GBM, glioblastoma; GelMA, gelatin methacryloyl; LCST, lower critical solution temperature; MMP, matrix metalloproteinase; NP, nanoparticle; PDAC, pancreatic ductal adenocarcinoma; PDO, patient-derived organoid; PEG, poly(ethylene glycol); PNIPAM, poly(N-isopropylacrylamide); RGD, arginine-glycine-aspartic acid; UCST, upper critical solution temperature.

4. Stimuli-Responsive Mechanisms in Cancer Bioinks

This section classifies the stimulus-responsive mechanisms engineered into bioinks. Three aspects receive particular emphasis: the underlying molecular chemistry, the tumor-relevant rationale for each stimulus, and the response kinetics and reversibility

that determine model utility. Figure 2 presents the mechanistic spectrum as a classification tree with chemical schematics.

4.1 Temperature-responsive systems

Thermoresponsive inks exploit lower critical solution temperature (LCST) behavior. PNIPAM-based systems collapse and gel near 32 °C, whereas Pluronic F127 gels at physiological temperature. Both sol–gel transitions are cytocompatible and reversible, which makes them well suited to printing workflows[65-67] (Figure 2B). Recent molecular designs have expanded this palette considerably, yielding dynamically thermoresponsive materials whose transition temperatures and hysteresis can be tuned and whose responses can be coupled to additional triggers[78]. In cancer modeling, thermal responsiveness serves two purposes: it provides temperature-controlled gelation during printing, and it permits studies of mild hyperthermia. Dual photo-/thermo-responsive inks further improve printability while preserving cell viability[79,80]. Fever and hyperthermia are clinically relevant perturbations. Thermoresponsive inks therefore also enable on-demand stiffness switching during long-term culture, so that thermal history becomes a controlled experimental variable[78,79].

Thermal exposure is quantifiable, which makes it a programmable input to a printed model rather than an incidental culture condition. Clinical practice expresses thermal exposure as cumulative equivalent minutes at a reference temperature of 43 °C, which converts an arbitrary temperature–time history into a single dosimetric value[81]. These quantities are also printing and culture parameters: heating amplitude, dwell time, and the interval between successive exposures are all operator-controlled, so a defined thermal dose can be delivered repeatedly to the same construct. Two features of this response are relevant to resistance modeling. Mild hyperthermia (40–43 °C) alters tumor perfusion and the tumor microenvironment at the doses used clinically as an adjunct to radiotherapy and chemotherapy. Heating also induces a heat-shock response that confers transient thermotolerance and is frequently accompanied by cross-resistance to cytotoxic drugs and radiation[81,82]. Both effects depend on the thermal dose

ACCEPTED PAPER

and on the interval between exposures, and both decay with time. Thermal resistance in a printed model is therefore a function of the regimen applied to it, rather than a fixed cellular property. A thermoresponsive ink can impose a defined thermal dose and a defined recovery interval within a single construct. Thermal resistance thereby becomes a programmable and measurable variable, adding a second axis of acquired resistance alongside drug exposure[78,79]. Such experiments remain phenomenological: a heating protocol can reproduce thermotolerance and its associated cross-resistance, but no printed model has yet been shown to predict the thermal dose at which resistance emerges in patients.

4.2 pH-responsive systems

The acidotic TME (pH 6.5–6.9) arises from glycolytic metabolism and provides an endogenous, cancer-selective stimulus[4,51]. Acid-labile bonds include imines, acetal linkages, and β-thiopropionate esters. Incorporated into crosslinkers or drug conjugates, they accelerate gel degradation and payload release at tumor pH[51,83,84] (Figure 2C). One critical design consideration deserves emphasis: the response window should match interstitial tumor pH rather than the strongly acidic endolysosomal compartment used in systemic drug delivery. This distinction determines whether a pH-responsive ink reports or perturbs the modeled microenvironment. Combined pH/ROS-responsive hydrogels have demonstrated synergistic chemo-photodynamic activity and are directly relevant to modeling therapy-induced microenvironmental change. For screening applications, pH-responsive inks can serve as built-in reporters of metabolic acidification. As printed tumor cells proliferate and acidify their surroundings, an acid-labile crosslinker converts the metabolic state into a measurable mechanical or release signal[51,84]. This reporter functionality is particularly valuable in resistance studies, where the timing of acidification relative to drug exposure can be read out as a surrogate for metabolic adaptation[4,51]. Notably, pH is itself spatially heterogeneous within a single construct: the proliferating, poorly perfused core is markedly more acidotic than the better-oxygenated rim, so an ink whose response window brackets interstitial pH

ACCEPTED PAPER

6.5–6.9 will report such intra-tumoral gradients rather than a single averaged value (see also Section 2.4).

4.3 Enzyme-responsive systems (MMP and cathepsins)

Enzyme-responsive inks exploit the overexpression of MMPs and cathepsins in invasive tumors[32]. MMP-cleavable peptide crosslinkers render hydrogels degradable by cell-mediated proteolysis, recapitulating the invasive front where cells remodel the matrix as they migrate[52,85] (Figure 2D). In bioprinted tumor microenvironments, proteolytic remodeling has been exploited to reproduce peritumoral matrix degradation and to study how degradation kinetics influence invasion[32]. Because MMP activity is both spatially heterogeneous and dynamically regulated, enzyme-responsive inks suit models in which matrix remodeling is coupled to cell behavior, a feature static inks cannot provide. The spatiotemporal pattern of gel degradation can itself serve as a readout of invasive capacity, converting the matrix into a sensor of tumor aggressiveness[32,52]. Enzyme-responsive systems also enable selective payload release in high-MMP zones, mirroring the biology of the invasive rim and supporting spatially resolved studies of drug action[85]. The invasive rim is precisely where drug penetration is most compromised and where cells acquire migratory and stem-like programs. Enzyme-responsive matrices thus couple two resistance-relevant variables, matrix remodeling and drug access, in a single experimental system[32,52].

4.4 Redox/ROS-responsive systems

Tumors exhibit elevated ROS, and chemotherapy and radiotherapy further amplify oxidative stress[27,28]. ROS-responsive chemistries include thioketal, boronate ester, and disulfide bonds, which cleave under oxidative conditions and provide a direct readout-and-response loop for therapy-induced oxidative challenge[28,84,86] (Figure 2E). These systems enable closed-loop simulation of the chemotherapy/radiotherapy–ROS axis. A printed model that stiffens or releases reporters in response to drug-induced ROS generation can thereby report the oxidative microenvironment in which resistance

ACCEPTED PAPER

develops[27,28]. Conversely, ROS-scavenging and oxygen-generating hydrogels serve as experimental controls and model the tumor-protective redox buffering observed in vivo[86,87]. The same boronate and disulfide chemistries can be arranged to either cleave, releasing cargo, or to scavenge, neutralizing ROS. The design space therefore permits both probing and perturbing the redox environment within a single platform[28,84,86]. Nanocomposite platforms further exploit the redox axis for drug penetration. In a representative study, ferritin-based hydrogels that responded to the tumor redox microenvironment promoted tumor penetration and chemoimmunotherapy efficacy. Redox-responsive design can therefore influence both model fidelity and therapeutic outcome[88].

4.5 Photo-responsive systems

Light offers high spatiotemporal precision for patterning printed constructs. Photocrosslinking of GelMA and methacryloyl-modified polymers is the most common strategy for stabilizing printed structures. Photodegradable groups such as o-nitrobenzyl moieties enable localized softening and channel formation after printing[2,54] (Figure 2F). Near-infrared (NIR) photothermal and photodynamic modalities add a therapeutic perturbation dimension and are useful for modeling photothermal therapy responses and light-triggered on-demand release. Light can be applied with micrometer resolution. Photo-responsive inks are therefore the primary tool for generating spatial heterogeneity within a single construct, whether stiffness gradients, patterned ligand presentation, or zoned degradation[54,89]. This spatial programmability is directly relevant to cancer modeling, where intratumoral heterogeneity in mechanics and signaling is a recognized driver of drug resistance[18,47]. Photo-responsive inks also enable time-stamped perturbations: a region of a construct can be softened, stiffened, or destroyed at a chosen time point. The operator can thereby model invasion, therapy-induced matrix remodeling, or surgical-like resection within the culture[54,89].

ACCEPTED PAPER

4.6 Magnetic, electrical, and ultrasound-responsive systems

Externally triggered systems provide non-invasive, operator-controlled perturbation. Magnetic nanoparticles embedded in inks enable anisotropic alignment, mechanical actuation, and magnetically guided on-demand release[55,56] (Figure 2G). Ultrasound-responsive inks exploit acoustic stimulation for non-invasive drug release and for mechanostimulation of embedded cells. Ultrasound also offers tissue-relevant penetration depth and has been used to trigger release from hydrogel depots[90-92]. Piezoelectric and electroactive inks allow electrical stimulation to modulate cell behavior, an emerging dimension for studying electro-mechanical coupling in neural and muscle-adjacent tumors[91,92]. The principal advantage of these modalities is temporal control: perturbations can be applied, withheld, or cycled without disturbing the culture, which enables longitudinal studies of adaptation and resistance[55,56]. Among exogenous triggers, ultrasound is distinguished by tissue-relevant penetration and by the capacity to focus energy within a printed construct without physical contact. These properties suit longitudinal regimens in which a model is repeatedly challenged while remaining inside a sealed culture device[90,92]. Such systems also support dose–response designs in which the same construct is challenged repeatedly, mirroring the cycles of chemotherapy administration that drive acquired resistance in patients[55,56].

4.7 Multi-stimuli and logic-gated responses

Biological microenvironments present multiple simultaneous signals, and single-stimulus inks oversimplify this reality. Multi-responsive inks combine orthogonal chemistries to execute sequential programs. An initial pH-triggered phase, for example, can be followed by a ROS-triggered phase, mimicking acidification followed by oxidative stress during therapy[84,93,94]. Logic-gated designs use AND/OR conditions to increase specificity and reduce off-target responses. A payload is released only when two conditions are simultaneously met, and a stiffening program is activated only under a defined combination of enzyme and pH[55,94] (Figure 2H). These designs move the field

ACCEPTED PAPER

from single-parameter responsiveness toward multi-parameter fidelity, which is essential for modeling the complex, layered signals of the evolving TME[12,36]. From an engineering standpoint, orthogonal chemistries must be selected with care so that their response windows do not overlap destructively. Their combined kinetics must also be validated under the actual culture conditions of the model. Validation should also include single-stimulus controls for each responsive pathway. Only by perturbing one pathway at a time can the contribution of each signal to the observed phenotype be attributed[36,84].

4.8 Mechanism comparison and selection strategy

Choosing among mechanisms requires matching response dynamics (minutes to days), reversibility, cytotoxicity, and printing compatibility to the biological question. Reversibility is selected by the process to be modeled rather than by ease of switching. Progressive fibrosis requires chemistry whose state change persists on the time scale of the experiment, which irreversible stiffening networks provide[12,29]. Processes that resolve after treatment require recoverable chemistry instead[55,56]. Table 2 provides a structured comparison across these dimensions. A general heuristic follows from the source of the trigger. Endogenous-stimulus inks (pH, enzyme, ROS) suit autonomous recapitulation of TME evolution. Exogenous-trigger inks (light, magnetic, ultrasound) suit hypothesis-driven perturbation studies, and hybrid systems combine both[36,56]. A final consideration is measurement compatibility. The chosen chemistry must not interfere with the screening readout, such as fluorescent reporters or interferometry, and its degradation products must not confound viability or omics assays[36,95]. Throughput further constrains mechanism choice for screening arrays. Stimuli that require external instrumentation, whether light, ultrasound, or magnetic fields, must be compatible with plate-scale parallel application. Endogenous-trigger inks self-respond without added infrastructure and are therefore favored in high-density array formats[95,96].

ACCEPTED PAPER

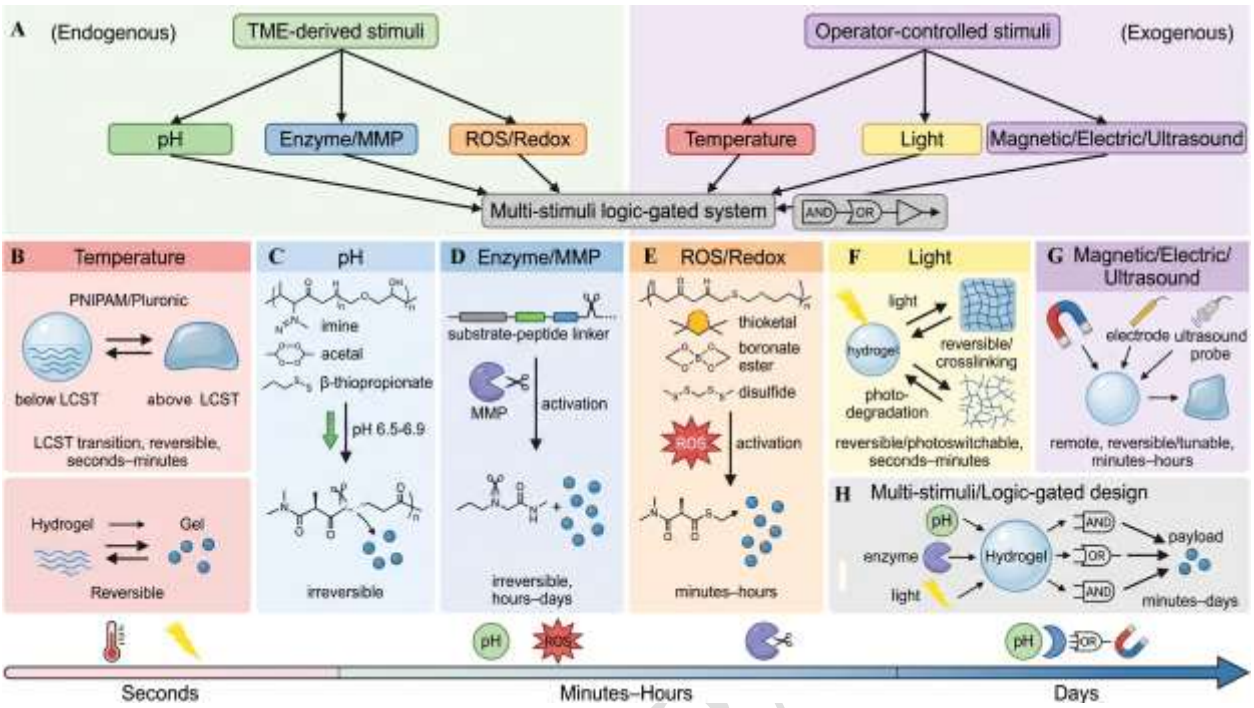


Figure 2. Spectrum of stimuli-responsive mechanisms in cancer bioinks. A, Classification tree separating endogenous (TME-derived: pH, enzyme, ROS/redox) and exogenous (operator-controlled: temperature, light, magnetic/electric/ultrasound) stimuli, and their integration into multi-stimuli logic-gated systems. B–G, Representative chemistries and response properties for temperature (B, poly(N-isopropylacrylamide) (PNIPAM)/Pluronic lower critical solution temperature (LCST) transition, seconds–minutes, reversible), pH (C, imine/acetal/β-thiopropionate cleavage at pH 6.5–6.9, minutes–hours, irreversible), enzyme/MMP (D, substrate-peptide linker cleavage, hours–days, irreversible), ROS/redox (E, thioketal/boronate ester/disulfide cleavage or scavenging, minutes–hours), light (F, photocrosslinking/photodegradation for spatial patterning, seconds–minutes, reversible/photoswitchable), and magnetic/electric/ultrasound (G, remote non-invasive activation, minutes–hours, reversible/tunable). H, Multi-stimuli and logic-gated designs (AND/OR/sequential programs) enable conditional release over minutes to days. The timeline at the bottom indicates typical response dynamics from seconds to days.

ACCEPTED P

Table 2. Comparison of stimuli-responsive mechanisms in cancer bioinks

Stimulus	Responsive chemistry	Representative ink examples	Tumor-relevant rationale	Response dynamics and reversibility	Key limitations
Temperature	LCST transition (PNIPAM, Pluronic F127); UCST (poly(N-acryloyl glycinamide))	PNIPAM-PEG; Pluronic-GelMA; thermoresponsive dECM	On-demand sol–gel transition for cell harvesting; temperature-triggered release; injectable delivery	Seconds – minutes; reversible	Narrow temperature window; potential cytotoxicity; limited mechanical strength; leaching
pH	Acid-labile bonds: imine, acetal, β-thiopropionate, boronate ester (low pH)	Acetal-crosslinked PEG; imine-dynamic hydrogels; boronate-HA; pH-sensitive alginate	Warburg acidosis (pH 6.5–6.9) triggers de-crosslinking or drug release in tumor interstitium	Minutes – hours; generally irreversible cleavage	Narrow pH window; off-target cleavage in normal acidic compartments (lysosomes); limited in vivo stability
Enzyme (MMP)	MMP-cleavable peptide linkers (GPQG↓IWGQ);	MMP-sensitive PEG; peptide-crosslinked HA; dECM with	MMP-2/9/14 overexpression in invasive front; models	Hours – days; irreversible	Enzyme concentration variability; broad

	cathepsin substrates	MMP motifs; MMP-GelMA	cell-mediated ECM remodeling and invasion		substrate specificity; batch-dependent kinetics; difficult to quantify
ROS / Redox	Thioketal cleavage; boronate ester oxidation; disulfide reduction	ROS-cleavable PEG; boronate-HA; disulfide-crosslinked gelatin; thioketal-PEG	Chemotherapy / radiotherapy-induced ROS elevation; mimics oxidative TME; ROS-triggered release or scavenging	Minutes – hours; cleavage or scavenging (design-dependent)	ROS background in culture media; glutathione interference; limited specificity; degradation product toxicity
Light	Photocrosslinking (methacrylate radical); photodegradation (o-nitrobenzyl, coumarin); photoisomerization (azobenzene)	GelMA; PEG-diacrylate; photodegradable PEG; azobenzene-modified HA	Spatially resolved patterning of stiffness and adhesion; non-invasive external control; high spatiotemporal precision	Seconds – minutes; reversible (photo-switchable) or irreversible (photocleavage)	UV cytotoxicity; limited tissue penetration (NIR improves); oxygen inhibition of radicals;

					equipment dependence
Magnetic / Electric / Sono	Magnetic NP (Fe_3O_4) actuation; conductive polymers (PEDOT:PSS); ultrasound cavitation	Magnetic NP-reinforced alginate; conductive GelMA; sono-responsive liposome-hydrogel	Remote non-invasive actuation; magnetic alignment for anisotropy; electrical stimulation for cell behavior; deep-tissue release	Minutes – hours; reversible / tunable	Magnetic field requirement; Joule heating (electrical); cavitation damage (ultrasound); NP clearance and long-term safety
Multi-stimuli and logic-gated	Orthogonal combinations: pH + enzyme, ROS + light, temperature + magnetic; AND / OR logic	Dual-responsive PNIPAM-boronate; MMP+pH logic-gated PEG; AND-gated release systems; logic-gated dECM	Mimics multifactorial TME; conditional release only when multiple stimuli coincide; improves specificity and fidelity	Minutes – days; depends on programmed logic	Chemistry complexity; potential interference between mechanisms; difficult validation; limited design rules

Abbreviations: dECM, decellularized extracellular matrix; GelMA, gelatin methacryloyl; HA, hyaluronic acid; LCST, lower critical solution temperature; MMP, matrix metalloproteinase; NIR, near-infrared; NP, nanoparticle; PEDOT:PSS, poly(3,4-ethylenedioxythiophene):poly(styrene sulfonate); PEG, poly(ethylene glycol); PNIPAM,

poly(N-isopropylacrylamide); ROS, reactive oxygen species; TME, tumor microenvironment; UCST, upper critical solution temperature; UV, ultraviolet.

5. Recapitulating the Dynamic TME with Smart Bioinks

5.1 Dynamic stiffness and viscoelastic remodeling

Matrix stiffening is a hallmark of desmoplastic tumors (Figure 3A). Its causal role in chemoresistance has been established in patient-derived pancreatic cancer organoids: organoids cultured in stiff matrices acquire resistance to gemcitabine through mechanotransductive signaling[29,30]. Matrix mechanics is therefore not merely correlative but mechanistically instructive. Desmoplastic tumors such as PDAC additionally overexpress crosslinking enzymes, notably LOX, whose activity is itself a therapeutic target; an engineered matrix that recapitulates LOX-mediated stiffening therefore reproduces both the mechanical state and the druggable biology of the disease[29,31]. Dynamic hydrogels now enable programmable stiffening and stress relaxation to mimic fibrosis progression and mechanical memory in culture[12,53,76]. Such systems allow experiments in which matrix stiffness is increased after an initial culture period, recapitulating the temporal sequence of desmoplasia, and testing whether resistance emerges only when stiffening precedes drug exposure[29,53]. The viscoelastic dimension adds further nuance. Engineered viscoelastic matrices have been shown to regulate invasion through Sp1-dependent mechanotransduction in breast cancer, indicating that both elastic stiffness and stress relaxation must be controlled to model resistance-relevant phenotypes[53,76]. The molecular effectors of this mechanosensing are increasingly well defined. Mechanosensitive ion channels such as Piezo1 transduce matrix mechanics into intracellular calcium and downstream transcriptional programs. Engineered matrices thus provide the controlled platform needed to interrogate which of these effectors dominates a given resistance phenotype[42,97].

In ovarian cancer, this dual control has now been quantitatively demonstrated: a 3D-bioprinted model in which graded extracellular matrix stiffening attenuated tumor-cell sensitivity to chemotherapy, providing direct experimental evidence that matrix

ACCEPTED PAPER

stiffness is a mechanistically instructive—not merely correlative—variable of resistance[98].

5.2 Oxygen and metabolic gradients

Hypoxia drives chemotherapy and immunotherapy resistance through HIF-dependent transcriptional programs, yet most printed models lack controlled oxygen gradients[27,99] (Figure 3B). Oxygen-generating inks and oxygen-scavenging components create and stabilize hypoxic cores that mimic in vivo pO2 gradients, enabling studies of hypoxia–HIF signaling, metabolic vulnerability, and hypoxia-induced immune evasion[100-102]. Microfluidic integration further sharpens oxygen and nutrient gradients. In a representative study,a hypoxia-integrated glioblastoma model demonstrated that oxygen gradients alone drive stemness, invasion, and temozolomide resistance, with the IC50 increasing by 56% under hypoxia[99,103]. Because metabolic gradients determine drug penetration and efficacy, their faithful reproduction is a prerequisite for any quantitative screening claim[27,103]. Beyond oxygen, chip-integrated models are being engineered to reproduce the full metabolic and pharmacokinetic context, including drug distribution and clearance. Printed tumor compartments thereby experience realistic exposure profiles. This integration is essential before resistance measurements can be compared quantitatively across patients[104,105].

5.3 On-demand delivery and spatiotemporal signaling

Smart inks function as programmable delivery systems within the model, releasing chemotherapeutics, immune agonists, or reporters on schedule. Sequential nanocomposite hydrogels that reprogram CAFs and logic-gated systems that release dual payloads in a defined order illustrate how release programming can recapitulate the temporally structured signaling of the TME[94,106] (Figure 3C). For screening platforms, controlled dose–time administration is essential: the same cumulative dose delivered gradually versus as a bolus can produce different resistance outcomes, and smart inks provide the temporal control required to test this[55,107,108]. The ability to

ACCEPTED PAPER

deliver a second stimulus after a defined interval, mimicking the sequencing of chemoradiation or induction–consolidation regimens, positions smart inks as tools for regimen optimization rather than single-agent IC50 measurement[94,106]. Delivery vehicles themselves can carry the signal. Extracellular-vesicle-loaded hydrogels provide programmable, biologically sourced release of signaling cargo, and stimuli-responsive micromotors add self-propelled, directional payload transport within a printed construct, extending on-demand delivery from bulk release toward anatomically structured presentation of cues[109,110]. Release programming also enables the sequential application of multiple agents, for example, priming, followed by the cytotoxic drug, followed by a checkpoint modulator, so that combination regimens can be screened in their clinical sequence rather than as simultaneous cocktails[94,106].

5.4 4D bioprinting and morphological dynamics: a conceptual future direction

Four-dimensional bioprinting, in which printed constructs undergo programmed shape changes over time, extends dynamic recapitulation from the molecular scale to the tissue scale[49,50,111](Figure 3D). The vast majority of 4D tumor-printing reports to date are materials demonstrations rather than biological studies: shape change is characterized in detail, but its consequences for drug-response phenotypes are rarely measured[111]. The rationale for pursuing this direction is therefore mechanistic rather than evidential. Matrix and tissue-scale mechanics are documented drivers of resistance-relevant phenotypes, and shape-changing constructs impose exactly this mechanical regime. Cyclic deformation, compaction, and release are candidate cues for dormancy entry and for the phenotypic transitions underlying resistance. Four-dimensional constructs would allow these cues to be applied, timed, and withdrawn under experimental control. Morphological readouts are similarly informative: the invasion budding, contraction, and morphological transitions that accompany epithelial–mesenchymal plasticity provide an observable signature of lineage switching[49,50].

ACCEPTED PAPER

Emerging dynamic chemistries supply the engineering substrate for such experiments. Dual-network hydrogels, in which one network is structurally stable and the other is exchangeable, enable time-stamped morphological experiments within a single printed system[75]. This review therefore positions 4D bioprinting as a conceptual future direction for cancer modeling: a hypothesis-generating tool for studying therapy-induced tissue-scale remodeling, not an established capability[111].

5.5 Vascularization and perfusion integration

Vascularization determines drug delivery, oxygen supply, and immune infiltration in tumors, and perfusion insufficiency directly fuels the hypoxia–resistance axis[27,112,113]. Prevascularized constructs, endothelial–tumor co-cultures, and perfusable chips have been fabricated by bioprinting sacrificial networks and self-assembling endothelial cells[112-115]. Integration of perfusion with smart inks is a key frontier: perfusable, dynamically remodeling models would close the loop between vascular function and resistance evolution[115,116]. For brain tumors, bioprinted glioma models that support endogenous vascularization have been established, and multilayered cerebrovascular conduits demonstrate that lumen geometry governs extravasation patterns. These findings argue for printing vascular architecture with patient-matched dimensions rather than relying on default geometries[115,116].

ACCEPTED PAPER

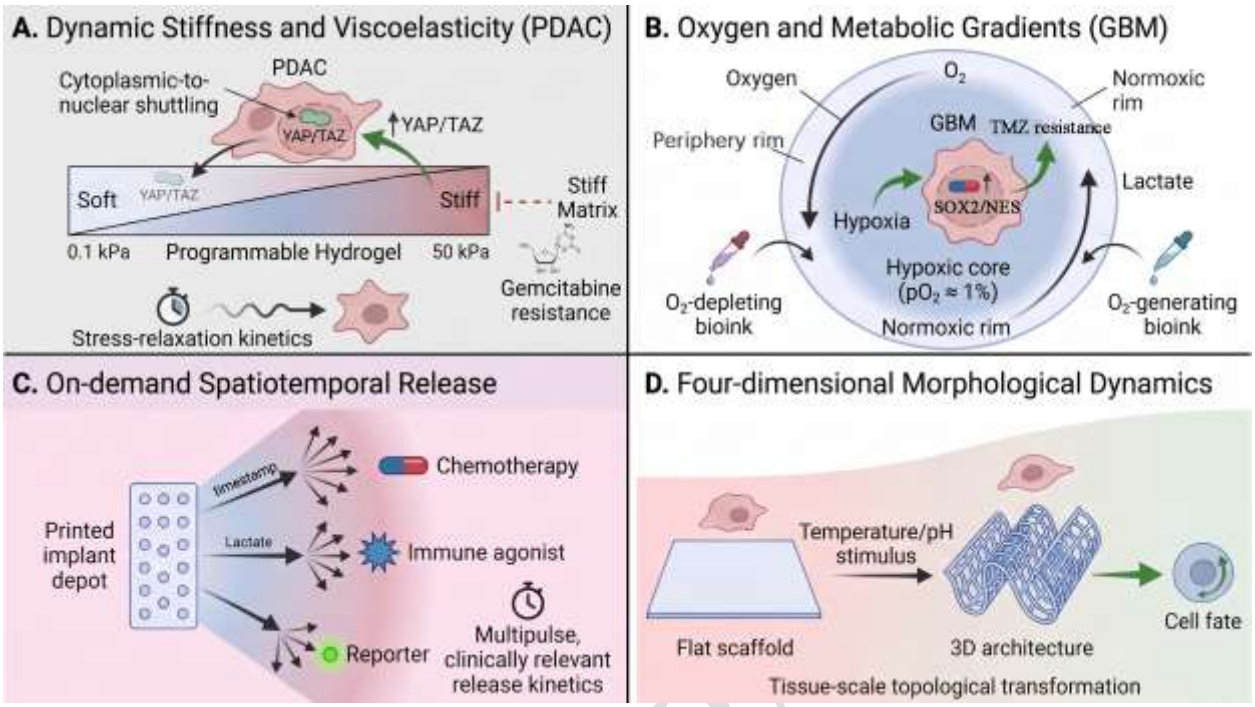


Figure 3. Recapitulating the dynamic tumor microenvironment with smart bioinks. A, Dynamic stiffness and viscoelasticity. Programmable soft-to-stiff transitions (0.1–50 kPa) drive YAP/TAZ mechanotransduction, whereas stress-relaxation kinetics modulate cell phenotype, exemplified by stiffness-mediated gemcitabine resistance in pancreatic ductal adenocarcinoma (PDAC). B, Oxygen and metabolic gradients. Oxygen-depleting or oxygen-generating bioinks establish hypoxic cores (pO2 ≈ 1%) surrounded by periphery rims and lactate gradients, recapitulating hypoxia-driven stemness, invasion, and temozolomide resistance in glioblastoma (GBM). C, On-demand spatiotemporal release. Printed depots enable the delivery of chemotherapeutics, immune agonists or reporters with multipulse, clinically relevant release kinetics, facilitating regimen-sequencing and combination studies. D, Four-dimensional morphological dynamics. Shape-memory folding and stress-driven morphing transform flat printed scaffolds into complex three-dimensional architectures triggered by stimuli such as temperature or pH, coupling tissue-scale topology with cell-fate decisions.

ACCEPTED

6. Applications in Drug Screening and Resistance Modeling

The ultimate test of smart-bioink tumor models lies in whether they improve therapeutic decision-making. This section evaluates their performance in high-throughput screening and, as the central theme of this review, their capacity to predict resistance phenotypes. This review anchors the discussion in PDAC, where stiffness-mediated

resistance is most completely documented. GBM serves as a complementary case for immune and vascularized models.

6.1 High-throughput and high-content drug screening platforms

Bioprinting has matured from proof-of-concept demonstrations into quantitative screening platforms. Single-organoid-resolution screening combines bioprinting with interferometric imaging, enabling label-free, time-resolved measurement of organoid responses across drug panels[95]. Automated spotters array 3D tumor spheroids at throughputs compatible with conventional high-throughput screening. High-throughput printed organoids of skin cancer have likewise been proposed for diagnosis and personalized therapy[96,117] (Figure 4B). The practical consequence is that screening campaigns can now run on patient-derived material at scale. Each printed construct consumes far fewer cells than conventional organoid assays, an advantage that matters when clinical specimens are limited[95,117]. The readout dimensions have correspondingly expanded beyond viability to morphology, protein secretion, and multi-omics. Spatially defined models now capture intratumoral heterogeneity as an explicit variable in screening[18,47,95] (Figure 4D). A distinctive advantage of printed arrays is standardization. Robotic deposition reduces the well-to-well variability that plagues manually seeded organoid assays, which improves the statistical power of dose–response comparisons[95,96]. Combined with smart inks, such arrays can additionally encode mechanical or chemical heterogeneity across the plate. This capability converts a screening campaign into a factorial experiment over both drug and microenvironmental variables[18,47] (Figure 4C). Two technical details determine whether such factorial screens are quantitatively reliable. First, the measurement modality must be compatible with the responsive ink. Label-free interferometric readouts avoid dye-related artifacts and can track organoid mass and morphology continuously over the culture window[95]. Second, array geometry must be standardized, because positional gradients in oxygen, pH, and mechanical support across a printed plate are themselves experimental variables. These variables must be characterized

ACCEPTED PAPER

before they can be controlled or exploited[95,96]. Early examples of such rigor include high-throughput printed skin-cancer organoid panels proposed for diagnosis and personalized therapy, in which plate-level quality metrics were integrated into the screening workflow[117].

Looking ahead, the convergence of bioprinting with microfluidic perfusion—enabled by hydrogel bioinks engineered simultaneously for printability and for efficient mass transport—is extending these plate-based factorial screens toward physiologically coupled, perfusable screening systems[118].

6.2 Treatment response and resistance prediction

Three levels of evidence must be distinguished when evaluating resistance prediction. Level (i) refers to the recapitulation of resistance-associated phenotypes in vitro. Level (ii) refers to retrospective correlation between model readouts and recorded clinical response. Level (iii) refers to prospective clinical prediction, in which model outputs anticipate resistance before it is clinically manifest. Current bioprinted cancer models operate predominantly at level (i), with level (ii) examples beginning to be reported in the organoid literature; no study has yet achieved level (iii)[12,48]. Clinical-correlation studies provide the Level (ii) evidence base for patient-derived models, linking model readouts to recorded treatment response. Personalized drug screening on patient-derived gastric cancer organoids showed clinical relevance with therapeutic outcomes. Organoid models of locally advanced or metastatic lung cancer predicted real-world tumor response. Colorectal cancer organoids with paired liver metastases recapitulated tumor heterogeneity and predicted chemotherapy response. Bladder cancer organoids, integrated with multi-omic characterization, revealed molecular correlates of gemcitabine response[5-8]. These studies validate the predictive potential of patient-derived culture systems and define the baseline against which bioprinted smart models must be judged. The organoid literature also clarifies the current ceiling of the field. Prediction of response to first-line therapy is approaching clinical utility. Prediction of

ACCEPTED PAPER

the trajectory toward resistance, that is, when and how a tumor will escape, remains largely unaddressed by static culture[48,119].

The added value of smart bioinks lies in making resistance itself the readout. Three mechanisms are especially amenable to prediction in dynamic models. The first is stiffness-mediated resistance. Stiff-matrix-cultured PDAC organoids develop gemcitabine resistance that is absent in soft matrices, implying that a stiffness-programmed printed model can predict resistance risk from matrix mechanics alone[29,30]. In the PDAC anchor case, the desmoplastic stroma produces a stiff, hypovascular, drug-impermeable niche. Engineered matrices that reproduce this stiffness have demonstrated both the mechanotransductive wiring (YAP/TAZ, integrin signaling) and the pharmacological consequence of reduced gemcitabine efficacy. These demonstrations provide a mechanistic template for stiffness-based resistance prediction[29,42,53]. The second is CSC enrichment and dormancy. Engineered dormancy-inducing matrices have uncovered mechanosensitive, drug-protective mechanisms such as FHL2-dependent survival. Hydrogel-based systems have likewise revealed the elusive cancer stem cells and dormancy states that static culture misses[44,45,120]. Brain vascular niche models capture glioblastoma infiltration, dormancy, and associated gene signatures in a single printed system. These models demonstrate that spatial niche reconstruction is sufficient to elicit dormant phenotypes[46]. The third is phenotypic plasticity. Progressive plasticity during metastasis and treatment persistence have been mapped in vivo. Dynamic matrices provide the controlled environment needed to probe which mechanical or biochemical cues trigger lineage switching[37,38,43]. The practical corollary is that resistance prediction requires not a single model but a small panel of models, each differing in one programmed variable at a time. This factorial design is one that printed arrays are uniquely positioned to deliver[18,95]. Critically, what has been demonstrated to date is the capacity to report resistance-correlated phenotypes. The prospective, patient-level validation that a bioprinted smart model predicts resistance before it occurs clinically remains the field's decisive open challenge[12,48].

ACCEPTED PAPER

A practical framework for resistance-prediction experiments emerges from these studies. The model should first reproduce the resistance-relevant microenvironmental state, including stiffness, hypoxia, and immune context, at baseline. It should then apply the therapeutic regimen with clinically matched dose–time schedules. Throughout the culture period, it should track dynamic readouts such as dormancy markers, CSC frequency, plasticity signatures, and matrix remodeling. Finally, it should map the observed phenotypic trajectory onto clinically defined resistance states. Each of these steps is directly supported by the smart-bioink strategies described in Section 3 and 4[12,46,48]. What is currently missing is the final, decisive step. This step is a prospective correlation of model-predicted resistance with patient outcomes, in cohorts large enough to establish predictive value. Such an analysis would be analogous to the retrospective studies that validated organoid response prediction[5,6,48].

Defining the predictive endpoint is the conceptual core of resistance prediction. In static assays, the endpoint is a single response value, such as an IC50 or an area under the dose–response curve, measured after a fixed incubation. In dynamic models, the informative endpoint is instead time-dependent, namely the trajectory along which sensitivity erodes. This review therefore proposes time-to-resistance as an organizing in vitro experimental endpoint (Figure 1D). This metric is defined as the time point at which a model's response to a clinically matched regimen falls below a predefined threshold. It is reported together with the identity of the resistance mechanism that emerges, whether stiffness-mediated, CSC-enriched, dormant, or plasticity-driven[12,37]. The organoid literature already provides the raw material for such trajectories. Long-term expandable patient-derived airway organoids established the technical basis for repeated-exposure studies. Beyond organoid systems, bioprinted glioblastoma models reconstructed from patient-derived cells have now enabled longitudinal preclinical assessment of CDK4/6 inhibition within a TME-faithful three-dimensional context—linking drug response to matrix mechanics, stromal signaling, and 28-day tumor growth kinetics in a single printed platform[121]. Longitudinal drug testing of lung-

ACCEPTED PAPER

cancer and digestive-system organoids has confirmed that repeated-exposure data are clinically informative even when analyzed with static endpoints[15,122-124]. What dynamic models add is the ability to attribute the trajectory to specific microenvironmental drivers. Each driver, including stiffness, hypoxia, acidosis, ROS, and immune pressure, can be programmed independently and in sequence[12,29]. The corresponding experimental design is a regimen-relevant stress test. The patient's cells are printed in a stiffness- and hypoxia-programmed ink and exposed to the clinical regimen at matched dose–time schedules. Resistance-correlated readouts, including dormancy markers, CSC frequency, plasticity signatures, and matrix remodeling, are monitored at intervals[46,48]. The output is not a binary sensitive/resistant call but a resistance-risk profile. This profile specifies the mechanism most likely to emerge, the anticipated time to escape under the programmed conditions, and the microenvironmental state most likely to accelerate it. Such information is hypothesis-generating until prospective validation is achieved; at present, it can inform the prioritization of regimens for testing, but not individual treatment decisions[8,48] (Figure 4E).

A final caveat concerns the interpretation of time-to-resistance. This metric is strictly an in vitro experimental endpoint. Its putative clinical counterparts are time-to-progression and time-to-treatment-failure under comparable exposure. The mapping between these quantities remains indirect. In vitro endpoints capture the kinetics of resistance emergence under controlled conditions, whereas clinical resistance onset additionally depends on patient-specific pharmacokinetics, immune context, and treatment history. In vitro time-to-resistance must therefore not be equated with the time of resistance onset in patients; the precise mapping, and its predictive value, remain to be established in prospective cohort studies[12,48].

6.3 Immunotherapy screening and immune–tumor co-culture

Immunotherapy has transformed oncology, and printed immune–tumor models are emerging as tools to predict immune checkpoint and cell-therapy responses. Early landmark work bioprinted glioblastoma microenvironments that model cellular

ACCEPTED PAPER

dependencies and immune interactions, establishing that printed constructs can recapitulate immune crosstalk[125]. Matrix mechanics directly modulate T-cell function. The mechanical properties of bioprinted hydrogels affect primary T-cell activation, and stiff immunosuppressive matrices dampen antitumor immunity, a variable that static soft cultures ignore[126]. CAR-T-cell screening on a bioprinted vascularized breast tumor model and genetic-engineering studies of CAR-T migration in bioprinted neuroblastoma models illustrate the use of printed platforms for cell-therapy optimization[127,128]. Macrophage–organoid co-cultures identify treatment strategies against macrophage-related chemoresistance. Organoid-on-a-chip systems predict immunotherapy responses in hepatocellular carcinoma. Organoid co-cultures probing systemic antitumor immunity in lung cancer extend the paradigm to systemic responses[129-131]. GBM is the anchor case for this axis. Its immunosuppressive TME, vascular co-option, and hypoxic core have been reproduced in printed and chip-based models, providing test beds for checkpoint blockade and cellular therapies[125,132-134]. The immune axis also introduces a cautionary variable. The biochemical quality of the model, down to endotoxin contamination of biomaterials, can alter macrophage–tumor interactions and therapeutic efficacy. This risk underscores the need for rigorous material quality control in immune-competent models[36,135]. Methodologically, the organoid–immune co-culture field provides protocols and quality standards that bioprinted platforms should inherit, including standardized tumor-organoid–T-cell co-culture assays and consensus guidance for organoid–immune interaction studies[136,137]. For GBM specifically, organoid models and bioprinted MSC–tumor co-cultures have begun to map the transcriptional consequences of stromal interaction. These studies reveal how non-immune stromal cells reshape the immune landscape, an axis that printed immune-competent GBM models will need to incorporate[138,139].

6.4 Integration of patient-derived models (PDO/PDX)

Patient-derived cells are the substrate on which predictive models are built. Bioprinted pancreatic cancer models derived from patient tissue preserve tumor–stroma

ACCEPTED PAPER

interactions and have been proposed as personalized therapy-testing platforms[48,140] (Figure 4A). Patient-derived renal cell carcinoma organoids have been printed for personalized therapy. Heterogeneous gallbladder carcinoma models capture intratumoral heterogeneity, and breast tumor–stroma models support preclinical drug testing. These examples collectively demonstrate the feasibility of multicellular, patient-specific constructs[141-144]. Immersion bioprinting of patient-derived brain tumor models in hyaluronan/collagen supports extends the approach to neural tumors[145]. The trajectory is from organoid spheres toward organoid systems, that is, printed constructs that integrate tumor, stroma, immune, and vascular compartments from the same patient. This configuration is the one most likely to carry predictive power into the clinic[48,119,131]. The parallel development of organoid biobanks linked to clinical annotations further accelerates this trajectory. Each banked specimen becomes a candidate for printing once its clinical outcome is known, enabling retrospective validation at scale[14,124]. The digestive-system organoid experience is instructive. Large cohorts of patient-derived organoids have been assembled specifically to support treatment decision-making. The quality-management principles developed for such cohorts, including tissue handling, culture fidelity checks, and clinical correlation, map directly onto bioprinted patient models[14,124].

Limitations of the bedside-to-bench-to-bedside workflow deserve explicit statement. First, patient-derived cells differ in expansion capacity and undergo culture drift over passages, which constrains repeated-exposure and longitudinal screening schemes. This variability also complicates the logistics of coordinating printing with surgical procurement and pathological diagnosis[48,119,140]. Second, intratumoral and interpatient heterogeneity means that a single specimen captures only a fraction of a tumor's clonal diversity. Clinically useful resistance-risk calls will therefore require multi-specimen panels and sample sizes beyond those of current proof-of-concept studies[119,141]. Third, the clinical-decision stage imposes requirements that preclinical workflows rarely meet: analytic validation of the readout, operation under certified quality systems of the

ACCEPTED PAPER

CLIA/CAP type, and a defined regulatory pathway for laboratory-developed tests. As discussed in Section 7.3, these requirements, not the printing technology itself, currently set the pace of translation[105,119,142].

The most recent embodiment of this configuration is the direct bioprinting of patient-derived cholangiocarcinoma organoid fragments within a decellularized liver matrix–based composite bioink, an approach that preserves native multicellular architecture while enabling standardized, image-based drug-response evaluation[143].

6.5 Local therapy and implantable scaffolds (complementary applications)

Beyond in vitro screening, smart-bioink platforms extend to local therapy and postsurgical recurrence prevention. 3D-printed implants loaded with therapeutics have been developed for glioblastoma treatment, and injectable hydrogels for postsurgical chemo-immunotherapy illustrate the same responsive chemistries deployed in vivo[83,146-148]. Conceptually, these local-delivery devices and the in vitro screening platforms share the same smart-ink logic. This shared logic creates the possibility of a closed loop. A patient's printed model screens the regimen, and an implantable responsive scaffold delivers the selected therapy[146,149]. This convergence is attractive for the special-issue theme of personalized cancer therapeutics, in which diagnosis, screening, and therapy are increasingly built on the same material and fabrication platforms[48,146]. The clinical readiness of such devices is suggested by in vivo studies of pH-responsive postoperative hydrogels and printed drug-loaded implants. These studies have demonstrated tolerability and local efficacy in animal models[83,146].

ACCEPTED PAPER

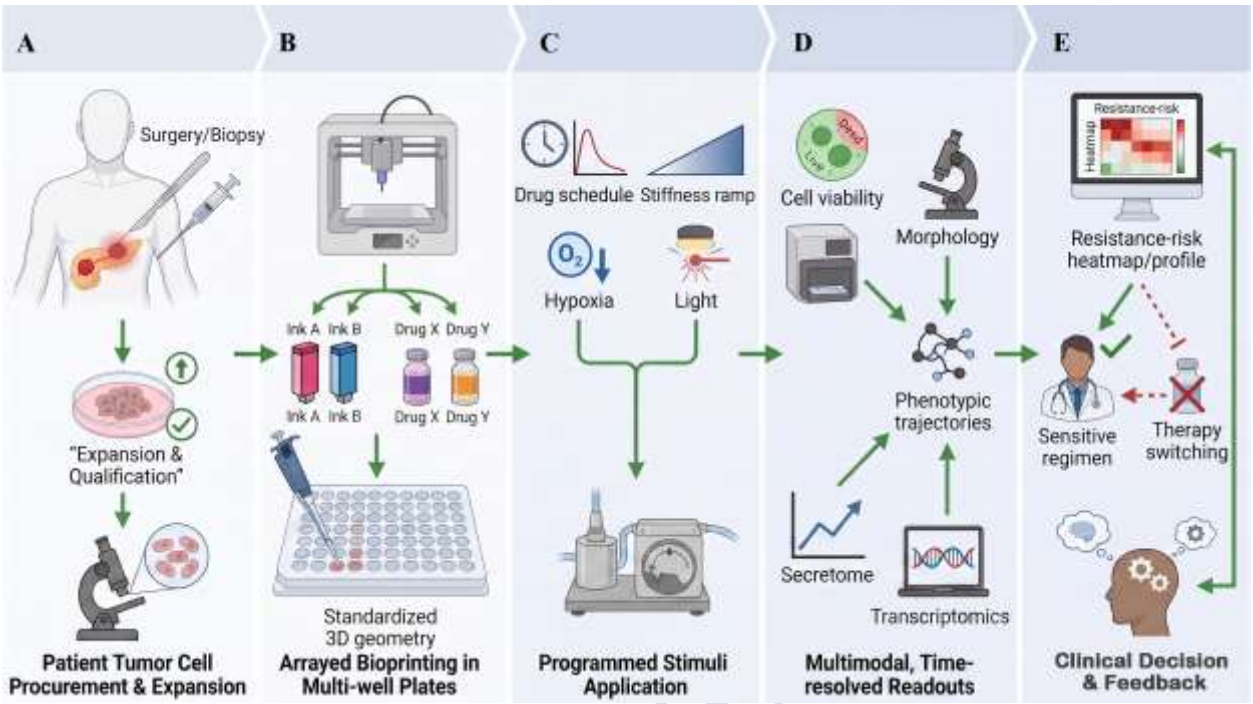


Figure 4. From patient-derived models to clinical decision: a predictive workflow. A, Patient-derived tumor cells are procured by surgery or biopsy, expanded, and qualified for printing. B, Arrayed bioprinting deposits factorial combinations of inks (for example, ink A versus ink B) and drugs (for example, drug X versus drug Y) into multi-well formats to standardize geometry and minimize well-to-well variability. C, Programmed endogenous or exogenous stimuli—including drug dose–time schedules, stiffness ramps, hypoxia, and light—are applied to match the clinical regimen. D, Multimodal, time-resolved readouts capture viability, morphology, secretome profiles and transcriptomics, generating phenotypic trajectories rather than single endpoints. E, The resulting resistance-risk profile informs clinical decision-making, distinguishing sensitive regimens from those requiring therapy switching (for example, gemcitabine/nab-paclitaxel in PDAC), and clinical outcomes feed back into iterative ink and protocol refinement. Limitations of this workflow—including patient-sample expansion capacity and heterogeneity, standardization prerequisites, and regulatory requirements—are discussed in Section 7.3.

7. Challenges and Future Perspectives

7.1 Engineering challenges

Four engineering gaps currently limit the fidelity of smart-bioink tumor models. The first is vascularization depth: most printed constructs lack perfusable vasculature beyond the first generations, which constrains the oxygen and drug-transport gradients that drive resistance[27,112,113]. Beyond the first few hundred micrometers of nutrient

diffusion, most printed constructs develop necrotic or hypoxic cores that are not physiologically structured; engineered perfusion must therefore be introduced early in culture, not as an end-stage feature[112,113]. The perfusion strategies reviewed in Section 5.5 address precisely this requirement. Delivery through the lumen, rather than by bulk diffusion, materially changes drug penetration and gradient profiles, and therefore the response readout[112-114]. The second is the stability of multi-mechanism responses: combining several responsive chemistries in one ink risks interference, premature activation, and irreproducible kinetics over long culture windows[36,84]. The third is matching response kinetics to experimental time scales: an ink that stiffens over hours cannot model desmoplasia that evolves over weeks, and vice versa[12,53].

For PDAC, desmoplasia accumulates over months of disease progression. The practical compromise is therefore to program a stiffness ramp spanning the culture window and to interpret results within that window, rather than claiming equivalence to the full clinical timeline[12,29]. The fourth is batch-to-batch reproducibility, particularly for dECM- and Matrigel-derived inks whose intrinsic variability propagates into model behavior[9,11]. These challenges are interdependent: improving vascularization without controlling matrix dynamics may produce models whose oxygen and mechanical histories are physiologically inconsistent, and vice versa[12,113].

7.2 Standardization and quality control

The clinical credibility of these models depends on standardization. Uniform protocols for mechanical characterization, defined benchmarks for response kinetics, and consensus nomenclature are prerequisites for cross-laboratory comparison[12,150,151].

Because dynamic models add time as an experimental dimension, reporting standards must also specify the observation window, the stimulus schedule, and the readout time points.

A stiffness value without its measurement history is as uninterpretable as a drug response without its dose-time protocol[12,36]. Parallel efforts in the organoid field, including consensus definitions for hepatic, pancreatic, and biliary organoids and

ACCEPTED PAPER

standardization frameworks for bone organoids, provide templates that bioprinted cancer models should adopt[150,151]. Validation must be anchored to clinical endpoints: a model's predictive claim is only as strong as the prospective patient-outcome correlation supporting it[5,119]. A pragmatic standardization roadmap would include (i) reference inks with certified mechanical and responsive properties; (ii) defined cell-density and printing-protocol standards; (iii) common readout protocols; and (iv) public benchmark datasets enabling algorithmic comparison of model performance[150,152]. A further practical measure is lot-level certification for commercial ink components, covering mechanical modulus, degradation rate, endotoxin level, and batch-to-batch variance, issued by suppliers and verified by end users, following the quality-by-design principles already applied in regulated manufacturing[135,150].

7.3 Clinical translation and regulatory pathways

Bringing bioprinted smart models into clinical use raises regulatory and ethical questions. In vitro diagnostic (IVD) and companion-diagnostic pathways, quality-management compliance (e.g., GCP-aligned workflows), and multicenter validation will be required before resistance modeling can inform treatment decisions[105,119]. From a quality-management perspective, the models must eventually operate under the same discipline as regulated diagnostics. This discipline entails defined specimen handling, documented assay performance, controlled reagent lots, and audit trails linking model output to clinical decisions. These requirements align with good clinical practice (GCP) and good manufacturing practice (GMP) expectations for any assay that informs patient care[105,150]. Importantly, such models are complements rather than substitutes for existing resistance diagnostics. Circulating tumor DNA (ctDNA) and comprehensive genomic profiling detect resistance when it is already present. In contrast, dynamic printed models aim to predict it prospectively by recapitulating the microenvironmental conditions under which resistance emerges[33,48]. The regulatory path is likely to begin with retrospective biobank studies, progress to prospective companion-diagnostic trials in defined indications (PDAC and GBM being natural candidates), and only then

ACCEPTED PAPER

generalize to broader oncology practice[48,105,119]. An attractive intermediate step is the retrospective model-the-trial design: take completed clinical trials whose patient specimens are biobanked, print the corresponding models under the trial's regimen, and ask whether the models would have predicted the observed responses. A positive retrospective result de-risks the prospective study and defines the assay's operating characteristics in advance[48,119].

7.4 AI and data fusion

Artificial intelligence is reshaping both ink design and model interpretation. Machine-learning approaches already optimize bioink formulations and printing parameters, and self-driving bioprinting laboratories are beginning to automate the design–print–measure loop[152-154]. AI-driven virtual organoids and digital twins, trained on printed-model and patient data, promise to simulate resistance trajectories and reduce experimental burden. The data loop is bidirectional: printed dynamic models generate the time-resolved perturbation data needed to train predictive algorithms, and those algorithms in turn guide the design of the next generation of inks. Interpretability is an underappreciated requirement: for a model whose output will inform therapy, clinicians need to understand which microenvironmental features drove the prediction, favoring algorithms that expose feature contributions rather than opaque black boxes[152,155]. A particularly promising convergence is the use of interferometric and label-free imaging to generate continuous, quantitative phenotype trajectories that serve directly as training data for resistance-prediction models[95,155]. The same trajectories can be generated across many patients in parallel, yielding the dataset scale that deep-learning approaches require. The remaining constraint is the availability of matched clinical outcomes to label those trajectories. This argues for biobank-linked prospective cohorts as the near-term priority[48,155].

8. Conclusion and future perspectives

ACCEPTED PAPER

Drug resistance in solid tumors is not a fixed property; it emerges from the dynamic interplay between tumor cells and a remodeling microenvironment. Static in vitro models capture tissue architecture at a single time point, yet they cannot reproduce the stiffening, acidification, hypoxia, oxidative stress, enzymatic remodeling, and immune re-education through which resistance evolves. Stimuli-responsive bioinks answer this need: they give bioprinted cancer models the capacity for controlled, biologically matched change over time. This review has traced the logic from microenvironmental blueprint to dynamic chemistry. This review classified the major responsive mechanisms and their selection criteria, surveyed strategies for recapitulating the dynamic TME, and weighed the evidence for where these models stand on the path from phenotype recapitulation to clinical prediction. Stiffness-programmed PDAC organoids and immune–vascular GBM models illustrate this transition. Current evidence remains proof-of-concept: the mechanisms are in place, resistance-associated phenotypes are demonstrable in printed models, and retrospective clinical correlation is emerging from the organoid literature, but prospective validation of resistance models in patients has not yet been achieved.

What remains is harder, and it is demanding but well defined. Dynamic materials must match biological time scales; model platforms must integrate perfusable vascularization, patient-matched stromal and immune compartments, and cross-laboratory standardization; and clinical translation must proceed through regulatory pathways that hold printed models to the same evidentiary standard as any diagnostic (Sections 7.1–7.4). This review therefore proposes a four-stage roadmap (Figure 5); the stages and their gating evidence are the authors' own projection, not a published consensus. Stage I (materials and phenotype fidelity) establishes responsive inks that reproduce resistance-associated phenotypes with lot-to-lot consistency. Stage II (vascularized and standardized models) requires perfusable vasculature, kinetic stability of multi-mechanism inks, and shared benchmarks before multicenter studies are meaningful. Stage III (predictive platform integration) couples AI-guided ink

ACCEPTED PAPER

formulation, self-driving laboratories, and immune-competent systems that integrate tumor, stroma, and immune compartments. Stage IV (clinical validation and adoption) proceeds from retrospective correlation in biobanked cohorts, through companion-diagnostic trials in anchor indications, to clinical adoption. Each transition is gated by the evidence of the preceding stage rather than by calendar time.

The practical near-term opportunities are concrete: stiffness-programmed PDAC models for gemcitabine/nab-paclitaxel response, immune-competent GBM models for checkpoint and CAR-T screening, and AI-guided ink formulation to compress the design cycle[29,125,154]. Each is achievable because the enabling pieces already exist: stiffness-programmable inks are commercially available, immune-competent GBM printing has been demonstrated, and closed-loop ink-optimization laboratories are operational. What is missing is their combination into a single, clinically annotated workflow[12,125,154]. If the roadmap milestones are met, dynamic patient-derived models may serve as personalized avatars: in vitro trial grounds in which a patient's tumor is printed, challenged, and interrogated before treatment begins[48,117]. The goal is no longer merely to print a tumor, but to print a tumor whose behavior can be anticipated. For the clinician, the promise is a model that answers the question asked before treatment begins: will this tumor respond under these microenvironmental conditions, or will it evolve resistance? For the engineer, the mandate is to build inks whose responses match biology at every scale, from bond kinetics to tissue perfusion. For the field, the challenge is collective: standardization, prospective validation, and honest reporting of what dynamic models can and cannot yet predict. Smart materials, bioprinting, patient-derived biology, and machine intelligence are now converging; the time is right to move decisively toward predictive, personalized cancer modeling.

ACCEPTED PAPER

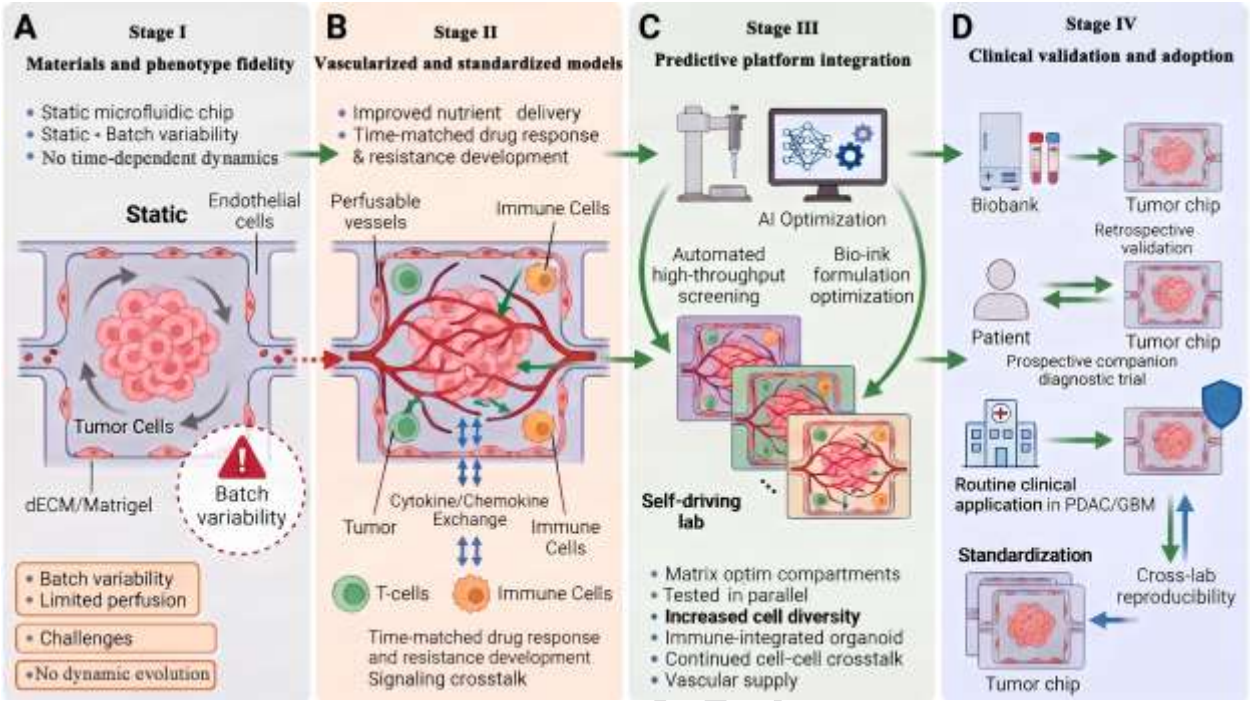


Figure 5.A proposed four-stage roadmap for bioprinted tumor models: from static descriptive systems to predictive, clinically validated diagnostics. This roadmap is a prospective projection proposed by the authors, not a published consensus. Stage transitions are gated by evidence rather than by calendar time. A, Stage I, materials and phenotype fidelity: the current baseline, in which static models lack time-dependent resistance, batch-to-batch variability in dECM/Matrigel inks remains uncontrolled, and vascularization depth and perfusion are limited. Advancing requires responsive inks that reproduce resistance-associated phenotypes with lot-to-lot consistency. B, Stage II, vascularized and standardized models: priority gaps include perfusable vasculature beyond the first generations, stability and cross-talk control of multi-mechanism responses, alignment of response kinetics with experimental timeframes, and cross-laboratory standardization frameworks, supported by AI-guided ink formulation and self-driving laboratories. C, Stage III, predictive platform integration: AI platforms and automation, immune-competent organoid systems that integrate tumor, stroma, and immune compartments, and self-driving optimization close the design–print–measure loop. D, Stage IV, clinical validation and adoption: retrospective biobank validation and companion-diagnostic trials converge on predictive diagnostic tools and clinical adoption in anchor indications such as PDAC and GBM. The overarching goal is the transition of bioprinted cancer models from descriptive surrogates to predictive, clinically validated diagnostics.

ACCEPTED P

Acknowledgments

None.

Funding

This work was supported by the Research Funds of Centre for Leading Medicine and Advanced Technologies of IHM (No. 2023IHM02003), the Clinical and Translational Research Project of Anhui Province (No. 202427b10020150), and the Anhui Provincial Health Commission Science and Technology Project (No. AHWJ2025BAm20013).

Conflict of interest

The authors declare no competing interests.

Author contributions

Conceptualization: Jing Zeng, Wei-Jian Ni

Funding acquisition: Wei-Jian Ni

Supervision: Wei-Jian Ni

Visualization: Jing Zeng

Writing–original draft: Jing Zeng

Writing–review & editing: Wei-Jian Ni

Ethics approval and consent to participate

Not applicable.

Consent for publication

Not applicable.

Availability of data

All data reviewed in this article are available from the cited references.

Further disclosure

During the preparation of this work, the authors used AI-assisted tools for language polishing. After using these tools, the authors reviewed and edited the content as needed and take full responsibility for the content of the publication.

ACCEPTED PAPER

References

1. Sharma R, Restan Perez M, da Silva VA, et al. 3D bioprinting complex models of cancer. *Biomaterials Science*. 2023;11(10):3414-3430. doi:10.1039/d2bm02060b
2. Datta P, Dey M, Ataie Z, Unutmaz D, Ozbolat IT. 3D bioprinting for reconstituting the cancer microenvironment. *npj Precision Oncology*. 2020;4(1):18. doi:10.1038/s41698-020-0121-2
3. Bahcecioglu G, Basara G, Ellis BW, Ren X, Zorlutuna P. Breast cancer models: Engineering the tumor microenvironment. *Acta Biomaterialia*. 2020;106:1-21. doi:10.1016/j.actbio.2020.02.006
4. Almazrouei KM, Mishra V, Pandya H, Sambhav K, Bhavsar SN. Tumor Microenvironment and Its Role in Cancer Progression: An Integrative Review. *Cureus*. 2025;17(9):e92707. doi:10.7759/cureus.92707
5. Zhao Y, Li S, Zhu L, et al. Personalized drug screening using patient-derived organoid and its clinical relevance in gastric cancer. *Cell Reports Medicine*. 2024;5(7):101627. doi:10.1016/j.xcrm.2024.101627
6. Wang H-M, Zhang C-Y, Peng K-C, et al. Using patient-derived organoids to predict locally advanced or metastatic lung cancer tumor response: A real-world study. *Cell Reports Medicine*. 2023;4(2):100911. doi:10.1016/j.xcrm.2022.100911
7. Mo S, Tang P, Luo W, et al. Patient-Derived Organoids from Colorectal Cancer with Paired Liver Metastasis Reveal Tumor Heterogeneity and Predict Response to Chemotherapy. *Advanced Science*. 2022;9(31):2204097. doi:10.1002/advs.202204097
8. Merrill NM, Kaffenberger SD, Bao L, et al. Integrative Drug Screening and Multiomic Characterization of Patient-derived Bladder Cancer Organoids Reveal Novel Molecular Correlates of Gemcitabine Response. *European Urology*. 2024;86(5):434-444. doi:10.1016/j.eururo.2024.05.026
9. Aisenbrey EA, Murphy WL. Synthetic alternatives to Matrigel. *Nature Reviews Materials*. 2020;5(7):539-551. doi:10.1038/s41578-020-0199-8
10. Kozlowski MT, Crook CJ, Ku HT. Towards organoid culture without Matrigel. *Communications Biology*. 2021;4(1):1387. doi:10.1038/s42003-021-02910-8
11. Zhao Z, Chen X, Dowbaj AM, et al. Organoids. *Nature Reviews Methods Primers*. 2022;2(1):94. doi:10.1038/s43586-022-00174-y
12. Zhang C, Shen Y, Huang M, et al. Dynamic hydrogel mechanics in organoid engineering: From matrix design to translational paradigms. *Bioactive Materials*. 2026;55:144-170. doi:10.1016/j.bioactmat.2025.09.021
13. Hofer M, Lutolf MP. Engineering organoids. *Nature Reviews Materials*. 2021;6(5):402-420. doi:10.1038/s41578-021-00279-y
14. Lv J, Du X, Wang M, Su J, Wei Y, Xu C. Construction of tumor organoids and their application to cancer research and therapy. *Theranostics*. 2024;14(3):1101-1125. doi:10.7150/thno.91362

ACCEPTED PAPER

15. Qu J, Kalyani FS, Liu L, Cheng T, Chen L. Tumor organoids: synergistic applications, current challenges, and future prospects in cancer therapy. *Cancer Communications*. 2021;41(12):1331-1353. doi:10.1002/cac2.12224
16. Lin M, Tang M, Duan W, Xia S, Liu W, Wang Q. 3D Bioprinting for Tumor Metastasis Research. *ACS Biomaterials Science & Engineering*. 2023;9(6):3116-3133. doi:10.1021/acsbiomaterials.3c00239
17. Matai I, Kaur G, Seyedsalehi A, McClinton A, Laurencin CT. Progress in 3D bioprinting technology for tissue/organ regenerative engineering. *Biomaterials*. 2020;226:119536. doi:10.1016/j.biomaterials.2019.119536
18. Yuan T, Fu X, Hu R, et al. Bioprinted, spatially defined breast tumor microenvironment models of intratumoral heterogeneity and drug resistance. *Trends in Biotechnology*. 2024;42(11):1523-1550. doi:10.1016/j.tibtech.2024.06.007
19. Romanazzo S, Tian P, Jalandhra GK, Doshi RB, Gooding JJ, Kilian KA. A biofabricated 3D cancer-stroma tumor microenvironment model. *Biofabrication*. 2025;17(4):045019. doi:10.1088/1758-5090/ae0a82
20. Xu K, Huang Y, Wu M, Yin J, Wei P. 3D bioprinting of multi-cellular tumor microenvironment for prostate cancer metastasis. *Biofabrication*. 2023;15(3):035020. doi:10.1088/1758-5090/acd960
21. Desigaux T, Comperat L, Dusserre N, et al. 3D bioprinted breast cancer model reveals stroma-mediated modulation of extracellular matrix and radiosensitivity. *Bioactive Materials*. 2024;42:316-327. doi:10.1016/j.bioactmat.2024.08.037
22. McCormack A, Highley CB, Leslie NR, Melchels FPW. 3D Printing in Suspension Baths: Keeping the Promises of Bioprinting Afloat. *Trends in Biotechnology*. 2020;38(6):584-593. doi:10.1016/j.tibtech.2019.12.020
23. Lian L, Xie M, Luo Z, et al. Rapid Volumetric Bioprinting of Decellularized Extracellular Matrix Bioinks. *Advanced Materials*. 2024;36(34):2304846. doi:10.1002/adma.202304846
24. Shi W, Mirza S, Kuss M, et al. Embedded Bioprinting of Breast Tumor Cells and Organoids Using Low-Concentration Collagen-Based Bioinks. *Advanced Healthcare Materials*. 2023;12(26):2300905. doi:10.1002/adhm.202300905
25. Agarwal T, Onesto V, Banerjee D, et al. 3D bioprinting in tissue engineering: current state-of-the-art and challenges towards system standardization and clinical translation. *Biofabrication*. 2025;17(4):042003. doi:10.1088/1758-5090/ade47a
26. Yigci D, Sarabi MR, Ustun M, et al. 3D bioprinted glioma models. *Progress in Biomedical Engineering*. 2022;4(4):042001. doi:10.1088/2516-1091/ac7833
27. Filipczak N, Joshi U, Attia SA, et al. Hypoxia-sensitive drug delivery to tumors. *Journal of Controlled Release*. 2022;341:431-442. doi:10.1016/j.jconrel.2021.11.034
28. Guo B, Yang F, Zhang L, et al. Cuproptosis Induced by ROS Responsive Nanoparticles with Elesclomol and Copper Combined with αPD-L1 for Enhanced Cancer Immunotherapy. *Advanced Materials*. 2023;35(22):2212267. doi:10.1002/adma.202212267

ACCEPTED PAPER

29. LeSavage BL, Zhang D, Huerta-López C, et al. Engineered matrices reveal stiffness-mediated chemoresistance in patient-derived pancreatic cancer organoids. *Nature Materials*. 2024;23(8):1138-1149. doi:10.1038/s41563-024-01908-x
30. Kalli M, Poskus MD, Stylianopoulos T, Zervantonakis IK. Beyond matrix stiffness: targeting force-induced cancer drug resistance. *Trends in Cancer*. 2023;9(11):937-954. doi:10.1016/j.trecan.2023.07.006
31. Saatci O, Kaymak A, Raza U, et al. Targeting lysyl oxidase (LOX) overcomes chemotherapy resistance in triple negative breast cancer. *Nature Communications*. 2020;11(1):2416. doi:10.1038/s41467-020-16199-4
32. Rasti Boroojeni F, Naeimipour S, Lifwergren P, et al. Proteolytic remodeling of 3D bioprinted tumor microenvironments. *Biofabrication*. 2024;16(2):025002. doi:10.1088/1758-5090/ad17d1
33. Kundu M, Butti R, Panda VK, et al. Modulation of the tumor microenvironment and mechanism of immunotherapy-based drug resistance in breast cancer. *Molecular Cancer*. 2024;23(1):92. doi:10.1186/s12943-024-01990-4
34. Chu X, Tian Y, Lv C. Decoding the spatiotemporal heterogeneity of tumor-associated macrophages. *Molecular Cancer*. 2024;23(1):150. doi:10.1186/s12943-024-02064-1
35. Finger A-M, Hendley AM, Figueroa D, Gonzalez H, Weaver VM. Tissue mechanics in tumor heterogeneity and aggression. *Trends in Cancer*. 2025;11(8):806-824. doi:10.1016/j.trecan.2025.04.004
36. Neumann M, di Marco G, Iudin D, et al. Stimuli-Responsive Hydrogels: The Dynamic Smart Biomaterials of Tomorrow. *Macromolecules*. 2023;56(21):8377-8392. doi:10.1021/acs.macromol.3c00967
37. Moorman A, Benitez EK, Cambuli F, et al. Progressive plasticity during colorectal cancer metastasis. *Nature*. 2024;637(8047):947-954. doi:10.1038/s41586-024-08150-0
38. Dhimolea E, de Matos Simoes R, Kansara D, et al. An Embryonic Diapause-like Adaptation with Suppressed Myc Activity Enables Tumor Treatment Persistence. *Cancer Cell*. 2021;39(2):240-256.e11. doi:10.1016/j.ccell.2020.12.002
39. Mao X, Xu J, Wang W, et al. Crosstalk between cancer-associated fibroblasts and immune cells in the tumor microenvironment: new findings and future perspectives. *Molecular Cancer*. 2021;20(1):131. doi:10.1186/s12943-021-01428-1
40. Nicolas AM, Pesic M, Engel E, et al. Inflammatory fibroblasts mediate resistance to neoadjuvant therapy in rectal cancer. *Cancer Cell*. 2022;40(2):168-184.e13. doi:10.1016/j.ccell.2022.01.004
41. Saraswathibhatla A, Indana D, Chaudhuri O. Cell–extracellular matrix mechanotransduction in 3D. *Nature Reviews Molecular Cell Biology*. 2023;24(7):495-516. doi:10.1038/s41580-023-00583-1
42. Villares E, Gerecht S. Engineered Biomaterials and Model Systems to Study YAP/TAZ in Cancer. *ACS Biomaterials Science & Engineering*. 2024;10(9):5550-5561. doi:10.1021/acsbiomaterials.4c01170

ACCEPTED PAPER

43. Laughney AM, Hu J, Campbell NR, et al. Regenerative lineages and immune-mediated pruning in lung cancer metastasis. *Nature Medicine*. 2020;26(2):259-269. doi:10.1038/s41591-019-0750-6
44. Sadra Bakhshandeh UH, Hubert M. Taïeb, Adithi R. Varadarajan, et al. Dormancy-inducing 3D engineered matrix uncovers mechanosensitive and drug-protective FHL2-p21 signaling axis. *Science Advances*. 2024;10(45):eadr3997. doi:10.1126/sciadv.adr3997
45. Melino S, Seliktar D. A hydrogel reveals an elusive cancer stem cell. *Cell Death & Disease*. 2021;12(5):415. doi:10.1038/s41419-021-03696-7
46. Lee VK, Tejero R, Silvia N, et al. 3D Brain Vascular Niche Model Captures Glioblastoma Infiltration, Dormancy, and Gene Signatures. *Advanced Science*. 2025;12(33):e00689. doi:10.1002/advs.202500689
47. McDonough E, Barroso M, Ginty F, Corr DT. Modeling intratumor heterogeneity in breast cancer. *Biofabrication*. 2024;17(1):012009. doi:10.1088/1758-5090/ad9b50
48. Vaskovich-Koubi D, Green Buzhor M, Krinsky A, et al. Patient-Derived 3D-Bioprinted Models of Pancreatic Cancer: Toward Personalized Therapy and Overcoming Tumor Microenvironment Challenges. *Advanced Drug Delivery Reviews*. 2025;225:115670. doi:10.1016/j.addr.2025.115670
49. Lai J, Liu Y, Lu G, et al. 4D bioprinting of programmed dynamic tissues. *Bioactive Materials*. 2024;37:348-377. doi:10.1016/j.bioactmat.2024.03.033
50. Faber L, Yau A, Chen Y. Translational biomaterials of four-dimensional bioprinting for tissue regeneration. *Biofabrication*. 2023;16(1):012001. doi:10.1088/1758-5090/acfdd0
51. Ding H, Tan P, Fu S, et al. Preparation and application of pH-responsive drug delivery systems. *Journal of Controlled Release*. 2022;348:206-238. doi:10.1016/j.jconrel.2022.05.056
52. Cook AB, Palange A, Schlich M, et al. Matrix metalloproteinase responsive hydrogel microplates for programmed killing of invasive tumour cells. *RSC Applied Polymers*. 2023;1(1):19-29. doi:10.1039/d3lp00057e
53. Lin F-Y, Chang C-Y, Nguyen H, Li H, Fishel ML, Lin C-C. Viscoelastic hydrogels for interrogating pancreatic cancer-stromal cell interactions. *Materials Today Bio*. 2023;19:100576. doi:10.1016/j.mtbio.2023.100576
54. Luo R, Xiang X, Jiao Q, Hua H, Chen Y. Photoresponsive Hydrogels for Tissue Engineering. *ACS Biomaterials Science & Engineering*. 2024;10(6):3612-3630. doi:10.1021/acsbiomaterials.4c00314
55. Alavi SE, Alharthi S, Alavi SZ, Raza A, Ebrahimi Shahmabadi H. Bioresponsive drug delivery systems. *Drug Discovery Today*. 2024;29(1):103849. doi:10.1016/j.drudis.2023.103849
56. Hu H, Busa P, Zhao Y, Zhao C. Externally triggered drug delivery systems. *Smart Materials in Medicine*. 2024;5(3):386-408. doi:10.1016/j.smaim.2024.08.004

ACCEPTED PAPER

57. de Barros NR, Gomez A, Ermis M, et al. Gelatin methacryloyl and Laponite bioink for 3D bioprinted organotypic tumor modeling. *Biofabrication*. 2023;15(4):045005. doi:10.1088/1758-5090/ace0db
58. Xu J, Yang S, Su Y, et al. A 3D bioprinted tumor model fabricated with gelatin/sodium alginate/decellularized extracellular matrix bioink. *International Journal of Bioprinting*. 2022;9(1):630. doi:10.18063/ijb.v9i1.630
59. Sekar MP, Suresh S, Zennifer A, Sethuraman S, Sundaramurthi D. Hyaluronic Acid as Bioink and Hydrogel Scaffolds for Tissue Engineering Applications. *ACS Biomaterials Science & Engineering*. 2023;9(6):3134-3159. doi:10.1021/acsbiomaterials.3c00299
60. Hauptstein J, Böck T, Bartolf-Kopp M, et al. Hyaluronic Acid-Based Bioink Composition Enabling 3D Bioprinting and Improving Quality of Deposited Cartilaginous Extracellular Matrix. *Advanced Healthcare Materials*. 2020;9(15):2000737. doi:10.1002/adhm.202000737
61. Kim HS, Lee KY. Stretchable and self-healable hyaluronate-based hydrogels for three-dimensional bioprinting. *Carbohydrate Polymers*. 2022;295:119846. doi:10.1016/j.carbpol.2022.119846
62. Zhu L, Yuhan J, Yu H, Zhang B, Huang K, Zhu L. Decellularized Extracellular Matrix for Remodeling Bioengineering Organoid's Microenvironment. *Small*. 2023;19(25):2207752. doi:10.1002/smll.202207752
63. De Santis MM, Alsafadi HN, Tas S, et al. Extracellular-Matrix-Reinforced Bioinks for 3D Bioprinting Human Tissue. *Advanced Materials*. 2020;33(3):2005476. doi:10.1002/adma.202005476
64. Xiang Y, Zhao Z, Yao EJ, et al. Multifaceted cancer alleviation by cowpea mosaic virus in a bioprinted ovarian cancer peritoneal spheroid model. *Biomaterials*. 2024;311:122663. doi:10.1016/j.biomaterials.2024.122663
65. Xu X, Liu Y, Fu W, et al. Poly(N-isopropylacrylamide)-Based Thermoresponsive Composite Hydrogels for Biomedical Applications. *Polymers*. 2020;12(3):580. doi:10.3390/polym12030580
66. Ansari MJ, Rajendran RR, Mohanto S, et al. Poly(N-isopropylacrylamide)-Based Hydrogels for Biomedical Applications: A Review of the State-of-the-Art. *Gels*. 2022;8(7):454. doi:10.3390/gels8070454
67. Navara AM, Kim YS, Xu Y, et al. A dual-gelling poly(N-isopropylacrylamide)-based ink and thermoreversible poloxamer support bath for high-resolution bioprinting. *Bioactive Materials*. 2022;14:302-312. doi:10.1016/j.bioactmat.2021.11.016
68. Träger A, Naeimipour S, Jury M, Selegård R, Aili D. Nanocellulose Reinforced Hyaluronan-Based Bioinks. *Biomacromolecules*. 2023;24(7):3086-3093. doi:10.1021/acs.biomac.3c00168
69. Kerch G. Nanocomposite Hydrogels and Extracellular Matrix—Advantages and Associated Risks. *Gels*. 2023;9(9):754. doi:10.3390/gels9090754

ACCEPTED PAPER

70. Li Q, Jiang Z, Ma L, et al. A versatile embedding medium for freeform bioprinting with multi-crosslinking methods. *Biofabrication*. 2022;14(3):035022. doi:10.1088/1758-5090/ac7909
71. Mueller E, Xu F, Hoare T. FRESH Bioprinting of Dynamic Hydrazone-Cross-Linked Synthetic Hydrogels. *Biomacromolecules*. 2022;23(11):4883-4895. doi:10.1021/acs.biomac.2c01046
72. Terriac L, Helesbeux J-J, Maugars Y, Guicheux J, Tibbitt MW, Delplace V. Boronate Ester Hydrogels for Biomedical Applications: Challenges and Opportunities. *Chemistry of Materials*. 2024;36(14):6674-6695. doi:10.1021/acs.chemmater.4c00507
73. Hull SM, Lou J, Lindsay CD, et al. 3D bioprinting of dynamic hydrogel bioinks enabled by small molecule modulators. *Science Advances*. 2023;9(13):eade7880. doi:10.1126/sciadv.ade7880
74. Cai C, Zhang X, Li Y, et al. Self-Healing Hydrogel Embodied with Macrophage-Regulation and Responsive-Gene-Silencing Properties for Synergistic Prevention of Peritendinous Adhesion. *Advanced Materials*. 2021;34(5):2106564. doi:10.1002/adma.202106564
75. Zhu M, Zhang H, Zhou Q, et al. Dynamic GelMA/DNA Dual-Network Hydrogels Promote Woven Bone Organoid Formation and Enhance Bone Regeneration. *Advanced Materials*. 2025;37(24):2501254. doi:10.1002/adma.202501254
76. Sharma A, Steger RF, Li JM, et al. Sp1 mechanotransduction regulates breast cancer cell invasion in engineered viscoelastic extracellular matrices. *Biomaterials*. 2026;327:123755. doi:10.1016/j.biomaterials.2025.123755
77. Jing S, Lian L, Hou Y, et al. Advances in volumetric bioprinting. *Biofabrication*. 2023;16(1):012004. doi:10.1088/1758-5090/ad0978
78. Kobayashi J, Nakayama M, Nagase K. Molecular design of dynamically thermoresponsive biomaterials. *Science and Technology of Advanced Materials*. 2025;26(1):2475736. doi:10.1080/14686996.2025.2475736
79. Moon SH, Park TY, Cha HJ, Yang YJ. Photo-/thermo-responsive bioink for improved printability in extrusion-based bioprinting. *Materials Today Bio*. 2024;25:100973. doi:10.1016/j.mtbio.2024.100973
80. Kim MH, Lin C-C. Norbornene-functionalized methylcellulose as a thermo- and photo-responsive bioink. *Biofabrication*. 2021;13(4):045023. doi:10.1088/1758-5090/ac24dc
81. Kok HP, van Rhoon GC, Herrera TD, Overgaard J, Crezee J. Biological modeling in thermoradiotherapy: present status and ongoing developments toward routine clinical use. *International Journal of Hyperthermia*. 2022;39(1):1126-1140. doi:10.1080/02656736.2022.2113826
82. Zhu W, Pan S, Zhang J, et al. The role of hyperthermia in the treatment of tumor. *Critical Reviews in Oncology/Hematology*. 2024;204:104541. doi:10.1016/j.critrevonc.2024.104541

ACCEPTED PAPER

83. Zhou J, Wang H, Chen H, et al. pH-responsive nanocomposite hydrogel for simultaneous prevention of postoperative adhesion and tumor recurrence. *Acta Biomaterialia*. 2023;158:228-238. doi:10.1016/j.actbio.2022.12.025
84. Yi D, Wang T, Xu S, et al. Injectable ROS/pH-Responsive Hydrogel for Synergistic Chemo-Photodynamic Tumor Therapy and Enhanced Wound Healing. *Advanced Healthcare Materials*. 2025;15(1):e02349. doi:10.1002/adhm.202502349
85. Yip AM-H, Lee LC-C, Shum J, Lo KK-W. A matrix metalloproteinase-responsive iridium(iii)-based hydrogel for cancer cell-specific imaging and lysosome-targeted photodynamic therapy. *Chemical Communications*. 2025;61(98):19461-19464. doi:10.1039/d5cc05380c
86. Sun H, Xu J, Wang Y, et al. Bone microenvironment regulative hydrogels with ROS scavenging and prolonged oxygen-generating for enhancing bone repair. *Bioactive Materials*. 2023;24:477-496. doi:10.1016/j.bioactmat.2022.12.021
87. Zhang W, Kuss M, Yan Y, Shi W. Dynamic Alginate Hydrogel as an Antioxidative Bioink for Bioprinting. *Gels*. 2023;9(4):312. doi:10.3390/gels9040312
88. Liu R, Liang Q, Luo JQ, et al. Ferritin-Based Nanocomposite Hydrogel Promotes Tumor Penetration and Enhances Cancer Chemoimmunotherapy. *Advanced Science*. 2023;11(3):2305217. doi:10.1002/advs.202305217
89. Zhong G, Miao Y, Zhou J, et al. Near-infrared light-induced photothermal and immunotherapy system for lung cancer bone metastasis treatment with simultaneous bone repair. *Bioactive Materials*. 2025;52:182-199. doi:10.1016/j.bioactmat.2025.06.008
90. Yeingst TJ, Arrizabalaga JH, Hayes DJ. Ultrasound-Induced Drug Release from Stimuli-Responsive Hydrogels. *Gels*. 2022;8(9):554. doi:10.3390/gels8090554
91. Xu D, Fu S, Zhang H, et al. Ultrasound-Responsive Aligned Piezoelectric Nanofibers Derived Hydrogel Conduits for Peripheral Nerve Regeneration. *Advanced Materials*. 2024;36(28):2307896. doi:10.1002/adma.202307896
92. Paci C, Iberite F, Arrico L, et al. Piezoelectric nanocomposite bioink and ultrasound stimulation modulate early skeletal myogenesis. *Biomaterials Science*. 2022;10(18):5265-5283. doi:10.1039/d1bm01853a
93. Dai F, Zhang J, Chen F, et al. A Multi-Responsive Hydrogel Combined With Mild Heat Stimulation Promotes Diabetic Wound Healing by Regulating Inflammatory and Enhancing Angiogenesis. *Advanced Science*. 2024;11(46):2408783. doi:10.1002/advs.202408783
94. Li S, Zheng W, Deng W, et al. Logic-Based Strategy for Spatiotemporal Release of Dual Extracellular Vesicles in Osteoarthritis Treatment. *Advanced Science*. 2024;11(26):2403227. doi:10.1002/advs.202403227
95. Tebon PJ, Wang B, Markowitz AL, et al. Drug screening at single-organoid resolution via bioprinting and interferometry. *Nature Communications*. 2023;14(1):3168. doi:10.1038/s41467-023-38832-8

ACCEPTED PAPER

96. Jeong M-H, Kim I, Park K, et al. An Automated High-Throughput Screening (HTS) Spotter for 3D Tumor Spheroid Formation. *International Journal of Molecular Sciences*. 2023;24(2):1006. doi:10.3390/ijms24021006
97. Wang J, Jing F, Zhao Y, You Z, Zhang A, Qin S. Piezo1: structural pharmacology and mechanotransduction mechanisms. *Trends in Pharmacological Sciences*. 2025;46(8):752-770. doi:10.1016/j.tips.2025.06.009
98. Shan Y, Pang M, Wang L, et al. Increased stiffness of extracellular matrix enhanced chemoresistance in 3D-bioprinted ovarian cancer model. *International Journal of Bioprinting*. 2024;10(3):1673. doi:10.36922/ijb.1673
99. Isik S, Yucel D, Hasirci V. Modeling a hypoxia-integrated glioblastoma microenvironment to mimic tumor heterogeneity and chemoresistance. *Biomaterials Science*. 2026;14(15):3963-3981. doi:10.1039/d5bm01824b
100. Montesdeoca CYC, Stocco TD, Marciano FR, Webster TJ, Lobo AO. 3D Bioprinting of Smart Oxygen-Releasing Cartilage Scaffolds. *Journal of Functional Biomaterials*. 2022;13(4):252. doi:10.3390/jfb13040252
101. Lu J-J, Zhang Q-C, Yuan G-C, et al. Oxygen-controllable injectable hydrogel alleviates intervertebral disc degeneration by balancing extracellular matrix metabolism. *Materials Today Bio*. 2024;29:101252. doi:10.1016/j.mtbio.2024.101252
102. Ntekoumes D, Song J, Liu H, Amelung C, Guan Y, Gerecht S. Acute Three-Dimensional Hypoxia Regulates Angiogenesis. *Advanced Healthcare Materials*. 2024;14(2):2403860. doi:10.1002/adhm.202403860
103. Ayuso JM, Rehman S, Farooqui M, et al. Microfluidic Tumor-on-a-Chip Model to Study Tumor Metabolic Vulnerability. *International Journal of Molecular Sciences*. 2020;21(23):9075. doi:10.3390/ijms21239075
104. Abed H, Radha R, Anjum S, et al. Targeted Cancer Therapy-on-A-Chip. *Advanced Healthcare Materials*. 2024;13(29):2400833. doi:10.1002/adhm.202400833
105. Monteduro AG, Rizzato S, Caragnano G, Trapani A, Giannelli G, Maruccio G. Organs-on-chips technologies - A guide from disease models to opportunities for drug development. *Biosensors and Bioelectronics*. 2023;231:115271. doi:10.1016/j.bios.2023.115271
106. Wang H, Chen Y, Wei R, et al. Synergistic Chemoimmunotherapy Augmentation via Sequential Nanocomposite Hydrogel-Mediated Reprogramming of Cancer-Associated Fibroblasts in Osteosarcoma. *Advanced Materials*. 2023;36(15):2309591. doi:10.1002/adma.202309591
107. Bayer IS. Hyaluronic Acid and Controlled Release: A Review. *Molecules*. 2020;25(11):2649. doi:10.3390/molecules25112649
108. Ciolacu DE, Nicu R, Ciolacu F. Cellulose-Based Hydrogels as Sustained Drug-Delivery Systems. *Materials*. 2020;13(22):5270. doi:10.3390/ma13225270
109. Ju Y, Hu Y, Yang P, Xie X, Fang B. Extracellular vesicle-loaded hydrogels for tissue repair and regeneration. *Materials Today Bio*. 2023;18:100522. doi:10.1016/j.mtbio.2022.100522

ACCEPTED PAPER

110. Zhou H, Dong G, Gao G, et al. Hydrogel-Based Stimuli-Responsive Micromotors for Biomedicine. *Cyborg and Bionic Systems*. 2022;2022:2022/9852853. doi:10.34133/2022/9852853
111. Wan Z, Zhang P, Liu Y, Lv L, Zhou Y. Four-dimensional bioprinting: Current developments and applications in bone tissue engineering. *Acta Biomaterialia*. 2020;101:26-42. doi:10.1016/j.actbio.2019.10.038
112. Han S, Kim S, Chen Z, et al. 3D Bioprinted Vascularized Tumour for Drug Testing. *International Journal of Molecular Sciences*. 2020;21(8):2993. doi:10.3390/ijms21082993
113. Miri AK, Khalilpour A, Cecen B, Maharjan S, Shin SR, Khademhosseini A. Multiscale bioprinting of vascularized models. *Biomaterials*. 2019;198:204-216. doi:10.1016/j.biomaterials.2018.08.006
114. Lee G, Kim SJ, Park JK. Fabrication of a self-assembled and vascularized tumor array via bioprinting on a microfluidic chip. *Lab on a Chip*. 2023;23(18):4079-4091. doi:10.1039/d3lc00275f
115. Wang X, Li X, Ding J, et al. 3D bioprinted glioma microenvironment for glioma vascularization. *Journal of Biomedical Materials Research Part A*. 2021;109(6):915-925. doi:10.1002/jbm.a.37082
116. Park W, Lee JS, Gao G, Kim BS, Cho DW. 3D bioprinted multilayered cerebrovascular conduits to study cancer extravasation mechanism related with vascular geometry. *Nature Communications*. 2023;14(1):7696. doi:10.1038/s41467-023-43586-4
117. Shukla AK, Shukla S, Suryawanshi SP, et al. High-Throughput 3D Bioprinted Organoids of Skin Cancer Utilized for Diagnosis and Personalized Therapy. *Current Oncology*. 2025;32(12):653. doi:10.3390/curroncol32120653
118. Li J, Li N, Liu B, Li S, Zhang H. Current advances of 3D-bioprinted microfluidic models with hydrogel bioinks and their applications in drug screening. *International Journal of Bioprinting*. 2024;10(3):1951. doi:10.36922/ijb.1951
119. Tong L, Cui W, Zhang B, et al. Patient-derived organoids in precision cancer medicine. *Med*. 2024;5(11):1351-1377. doi:10.1016/j.medj.2024.08.010
120. Li F, Li Z, Wei C, et al. Application of hydrogels for targeting cancer stem cells in cancer treatment. *Biomedicine & Pharmacotherapy*. 2024;180:117486. doi:10.1016/j.biopha.2024.117486
121. Kaps P, Zunke E, Ramtke J, et al. 3D bioprinting of the glioblastoma microenvironment for preclinical assessment of CDK4/6 inhibition. *Int J Bioprint*. 2026;12(2):025520537. doi:10.36922/ijb025520537
122. Sachs N, Papaspyropoulos A, Zomer-van Ommen DD, et al. Long-term expanding human airway organoids for disease modeling. *EMBO J*. 2019;38(4):EMBJ2018100300. doi:10.15252/embj.2018100300
123. Shi R, Radulovich N, Ng C, et al. Organoid Cultures as Preclinical Models of Non-Small Cell Lung Cancer. *Clinical Cancer Research*. 2020;26(5):1162-1174. doi:10.1158/1078-0432.Ccr-19-1376

ACCEPTED PAPER

124. Wang Y, Zhang L, Wang LZ, et al. The application of organoids in treatment decision-making for digestive system cancers: progress and challenges. *Molecular Cancer*. 2025;24(1):222. doi:10.1186/s12943-025-02429-0
125. Tang M, Xie Q, Gimple RC, et al. Three-dimensional bioprinted glioblastoma microenvironments model cellular dependencies and immune interactions. *Cell Research*. 2020;30(10):833-853. doi:10.1038/s41422-020-0338-1
126. Joseph JP, Gugulothu SB, Nandi D, Chatterjee K. Mechanical Properties Affect Primary T Cell Activation in 3D Bioprinted Hydrogels. *ACS Macro Letters*. 2023;12(8):1085-1093. doi:10.1021/acsmacrolett.3c00271
127. Dey M, Kim MH, Dogan M, et al. Chemotherapeutics and CAR-T Cell-Based Immunotherapeutics Screening on a 3D Bioprinted Vascularized Breast Tumor Model. *Advanced Functional Materials*. 2022;32(52):2203966. doi:10.1002/adfm.202203966
128. Andersch L, Grunewald L, Stecklum M, et al. Investigating genetic modifications to enhance L1CAM-CAR T cell migration in solid tumors in a 3D bioprinted neuroblastoma model. *Frontiers in Immunology*. 2025;16:1677361. doi:10.3389/fimmu.2025.1677361
129. Jiang S, Deng T, Cheng H, et al. Macrophage-organoid co-culture model for identifying treatment strategies against macrophage-related gemcitabine resistance. *Journal of Experimental & Clinical Cancer Research*. 2023;42(1):199. doi:10.1186/s13046-023-02756-4
130. Zou Z, Lin Z, Wu C, et al. Micro-Engineered Organoid-on-a-Chip Based on Mesenchymal Stromal Cells to Predict Immunotherapy Responses of HCC Patients. *Advanced Science*. 2023;10(27):2302640. doi:10.1002/advs.202302640
131. Li K, Liu C, Sui X, et al. An organoid co-culture model for probing systemic anti-tumor immunity in lung cancer. *Cell Stem Cell*. 2025;32(8):1218-1234.e7. doi:10.1016/j.stem.2025.05.011
132. Xie Z, Chen M, Lian J, Wang H, Ma J. Glioblastoma-on-a-chip construction and therapeutic applications. *Frontiers in Oncology*. 2023;13:1183059. doi:10.3389/fonc.2023.1183059
133. Ustun M, Rahmani Dabbagh S, Ilci I, Bagci-Onder T, Tasoglu S. Glioma-on-a-Chip Models. *Micromachines*. 2021;12(5):490. doi:10.3390/mi12050490
134. Pasupuleti V, Vora L, Prasad R, Nandakumar DN, Khatri DK. Glioblastoma preclinical models: Strengths and weaknesses. *Biochimica et Biophysica Acta (BBA) - Reviews on Cancer*. 2024;1879(1):189059. doi:10.1016/j.bbcan.2023.189059
135. Heinrich MA, Heinrich L, Ankone MJK, Vergauwen B, Prakash J. Endotoxin contamination alters macrophage-cancer cell interaction and therapeutic efficacy in pre-clinical 3D in vitro models. *Biomaterials Advances*. 2023;144:213220. doi:10.1016/j.bioadv.2022.213220
136. Cattaneo CM, Dijkstra KK, Fanchi LF, et al. Tumor organoid-T-cell coculture systems. *Nature Protocols*. 2020;15(1):15-39. doi:10.1038/s41596-019-0232-9
137. Magré L, Verstegen MMA, Buschow S, van der Laan LJW, Peppelenbosch M, Desai J. Emerging organoid-immune co-culture models for cancer research: from

ACCEPTED PAPER

oncoimmunology to personalized immunotherapies. *Journal for ImmunoTherapy of Cancer*. 2023;11(5):e006290. doi:10.1136/jitc-2022-006290
138. Wang X, Sun Y, Zhang DY, Ming G-l, Song H. Glioblastoma modeling with 3D organoids: progress and challenges. *Oxford Open Neuroscience*. 2023;2:kvad008. doi:10.1093/oons/kvad008
139. Oliver L, Landais Y, Gratas C, et al. Transcriptional landscape of the interaction of human Mesenchymal Stem Cells with Glioblastoma in bioprinted co-cultures. *Stem Cell Research & Therapy*. 2024;15(1):424. doi:10.1186/s13287-024-04022-6
140. Sun H, Wang Y, Sun M, et al. Developing Patient-Derived 3D-Bioprinting models of pancreatic cancer. *Journal of Advanced Research*. 2025;74:165-174. doi:10.1016/j.jare.2024.09.011
141. Mao S, Xie R, Shou J, Pang Y, Sun W. Bioprinting of patient-derived heterogeneous renal cell carcinoma organoids for personalized therapy. *Biofabrication*. 2025;17(4):045008. doi:10.1088/1758-5090/adecc5
142. Jin Y, Zhang J, Xing J, et al. Multicellular 3D bioprinted human gallbladder carcinoma forin vitromimicry of tumor microenvironment and intratumoral heterogeneity. *Biofabrication*. 2024;16(4):045028. doi:10.1088/1758-5090/ad6d8c
143. González-Callejo P, Vázquez-Aristizabal P, García-Astrain C, et al. 3D bioprinted breast tumor-stroma models for pre-clinical drug testing. *Materials Today Bio*. 2023;23:100826. doi:10.1016/j.mtbio.2023.100826
144. Yan Q, Hu W, Wang J, et al. 3D bioprinting of patient-derived cholangiocarcinoma organoids in a decellularized liver matrix-based bioink for drug testing. *Int J Bioprint*. 2026;12(3):026200188. doi:10.36922/ijb026200188
145. Clark CC, Yoo KM, Sivakumar H, et al. Immersion bioprinting of hyaluronan and collagen bioink-supported 3D patient-derived brain tumor organoids. *Biomedical Materials*. 2022;18(1):015014. doi:10.1088/1748-605X/aca05d
146. Korelidou A, Domínguez-Robles J, Islam R, Donnelly RF, Coulter JA, Larrañeta E. 3D-printed implants loaded with acriflavine for glioblastoma treatment. *International Journal of Pharmaceutics*. 2024;665:124710. doi:10.1016/j.ijpharm.2024.124710
147. Liu Z, Yin J, Qiu T, et al. Reversing the immunosuppressive tumor microenvironment via "Kynurenine starvation therapy" for postsurgical triple-negative breast cancer treatment. *Journal of Controlled Release*. 2025;383:113832. doi:10.1016/j.jconrel.2025.113832
148. Tsen HT, Sun TC, Lai TK, et al. Cisplatin-activated and hemoglobin-mediated injectable hydrogel system for antitumor chemodynamic and chemotherapy. *Biomedicine & Pharmacotherapy*. 2024;175:116713. doi:10.1016/j.biopha.2024.116713
149. Li X, Xu X, Xu M, Geng Z, Ji P, Liu Y. Hydrogel systems for targeted cancer therapy. *Frontiers in Bioengineering and Biotechnology*. 2023;11:1140436. doi:10.3389/fbioe.2023.1140436

ACCEPTED PAPER

150. Wang J, Chen X, Li R, et al. Standardization and consensus in the development and application of bone organoids. *Theranostics*. 2025;15(2):682-706. doi:10.7150/thno.105840
151. Marsee A, Roos FJM, Verstegen MMA, et al. Building consensus on definition and nomenclature of hepatic, pancreatic, and biliary organoids. *Cell Stem Cell*. 2021;28(5):816-832. doi:10.1016/j.stem.2021.04.005
152. Zhou C, Liu C, Liao Z, Pang Y, Sun W. AI for biofabrication. *Biofabrication*. 2024;17(1):012004. doi:10.1088/1758-5090/ad8966
153. Freeman S, Calabro S, Williams R, Jin S, Ye K. Bioink Formulation and Machine Learning-Empowered Bioprinting Optimization. *Frontiers in Bioengineering and Biotechnology*. 2022;10:913579. doi:10.3389/fbioe.2022.913579
154. Liu S, Kaur N, Song D-H, Moses JC, Ozbolat IT. Self-driving bioprinting laboratories. *Biofabrication*. 2026;18(1):013001. doi:10.1088/1758-5090/ae3645
155. Bai L, Su J. Artificial Intelligence Virtual Organoids (AIVOs). *Bioactive Materials*. 2026;59:45–68. doi:10.1016/j.bioactmat.2025.12.030

ACCEPTED PAPER